PRESSURE DISTRIBUTION ON AN AIRFOIL IN OSCILLATING FLOW

by

Terry Jon Allen

United States
Naval Postgraduate School

THESIS

PRESSURE DISTRIBUTION ON AN AIRFOIL

IN OSCILLATING FLOW

by

Terry Jon Allen

June 1969

Pressure Distribution on an Airfoil in Oscillating Flow

by

Terry Jon Allen
Lieutenant (junior grade), United States Navy
B.S., United States Naval Academy, 1968

Submitted in partial fulfillment of the
requirements for the degree of

MASTER OF SCIENCE IN AERONAUTICAL ENGINEERING

from the

NAVAL POSTGRADUATE SCHOOL
June 1969

ABSTRACT

The effect of oscillating flow on the pressure distribution of a symmetrical airfoil was investigated experimentally employing a remote pressure transducer.

An open circuit wind tunnel utilizing rotating shutter blades downstream of the test section was used to create oscillating flow. Tests were run at two frequencies, as well as at steady flow, and three angles of attack.

The mean and unsteady pressure characteristics were recorded from which mean values of the normal force were determined. The results indicate that an airfoil at high angle of attack will produce more lift in oscillating flow than in steady flow.

TABLE OF CONTENTS

LIST OF TABLES

LIST OF ILLUSTRATIONS

LIST OF SYMBOLS

Symbol	Definition	Units
α	Angle of Attack	degrees
C_n	Normal Force Coefficient	
C_p	Mean Pressure Coefficient	
x	Distance Downstream of Leading Edge	
c	Chord Length	
P_{sl}	Local Static Pressure	psia
P_{atm}	Atmospheric Pressure	psia
q	Dynamic Pressure	psia
$C_{p_{stag}}$	Stagnation Mean Pressure Coefficient	
C'_p	Root Mean Square Pressure Coefficient	
P_{rms}	Root Mean Square Pressure	psia
f	Frequency of Freestream Velocity Fluctuations	cps

ACKNOWLEDGMENTS

Tne author wishes to express his gratitude to Dr. James A. Miller, Department of Aeronautics, for his guidance and support during the present work.

Grateful recognition is also due Prof. L. V. Schmidt for his design of the remote pressure transducer and his advice regarding calibration procedures.

The author also wishes to express his appreciation to LCDR. R. Despard, USN, Doctorate Program, for his advice and suggestions.

I. INTRODUCTION

With the advent of the helicopter, there has been a need for a comprehensive study of the phenomenon associated with an airfoil in oscillating flow. A helicopter rotor blade is unique in that it experiences sinusoidal changes in velocity due to forward motion. Some work has been reported on airfoils in unsteady motion due to pitch and flapping, but due to restrictions on most wind tunnels, there has been little done in an oscillating free stream.

Greenberg [Ref. 1] presented an analysis predicting the forces on an airfoil in pitch oscillation. His paper followed one by Isaacs [Ref. 2] who had used linear theory to examine the same problem.

Liiva [Ref. 3] and later Liiva and Davenport [Ref. 4] made extensive investigations with a model which had the capability of cyclic changes in pitch and of cyclic plunging motions. They were concerned with the dynamic stall characteristics of rotor blades.

The objective of the present work was to analyze the mean and unsteady pressure characteristics of an airfoil in oscillating flow. Mean pressure distributions in unsteady flow, measured in a manner developed by Bergh and Tijdeman [Ref. 5], were compared with those in steady flow.

II. EXPERIMENTAL EQUIPMENT AND PROCEDURES

A. EQUIPMENT

1. General

The experimental work reported here was carried out in the Oscillating Flow Facilities of the Naval Postgraduate School.

2. The Wind Tunnel

The oscillating flow wind tunnel is an open circuit tunnel. Its test section is 24 inches square by 223 inches long having extremely stiff walls of metal and plastic.

Mean velocities up to 250 feet per second may be obtained from the two 100 horsepower Joy-Axivane fans. A typical velocity profile in steady flow is shown in Figure 1. A sinusoidal component is introduced into the free stream velocity by means of harmonic solid blockage variations that are introduced into the flow by means of four rotating shutter blades that horizontally span the tunnel at the trailing edge of the test section. A variable-speed motor controls the frequency of oscillation while amplitudes are determined by the widths of the shutter blades. Frequencies from 0.1 to 250 cycles per second may be produced. The 4-inch blades used in this investigation (Fig. 2) produced fluctuation amplitudes of 10 to 24% of the free-stream mean velocity. Reference 7 contains a complete description of the tunnel and its operation. Figure 3 is a schematic layout of the wind tunnel system.

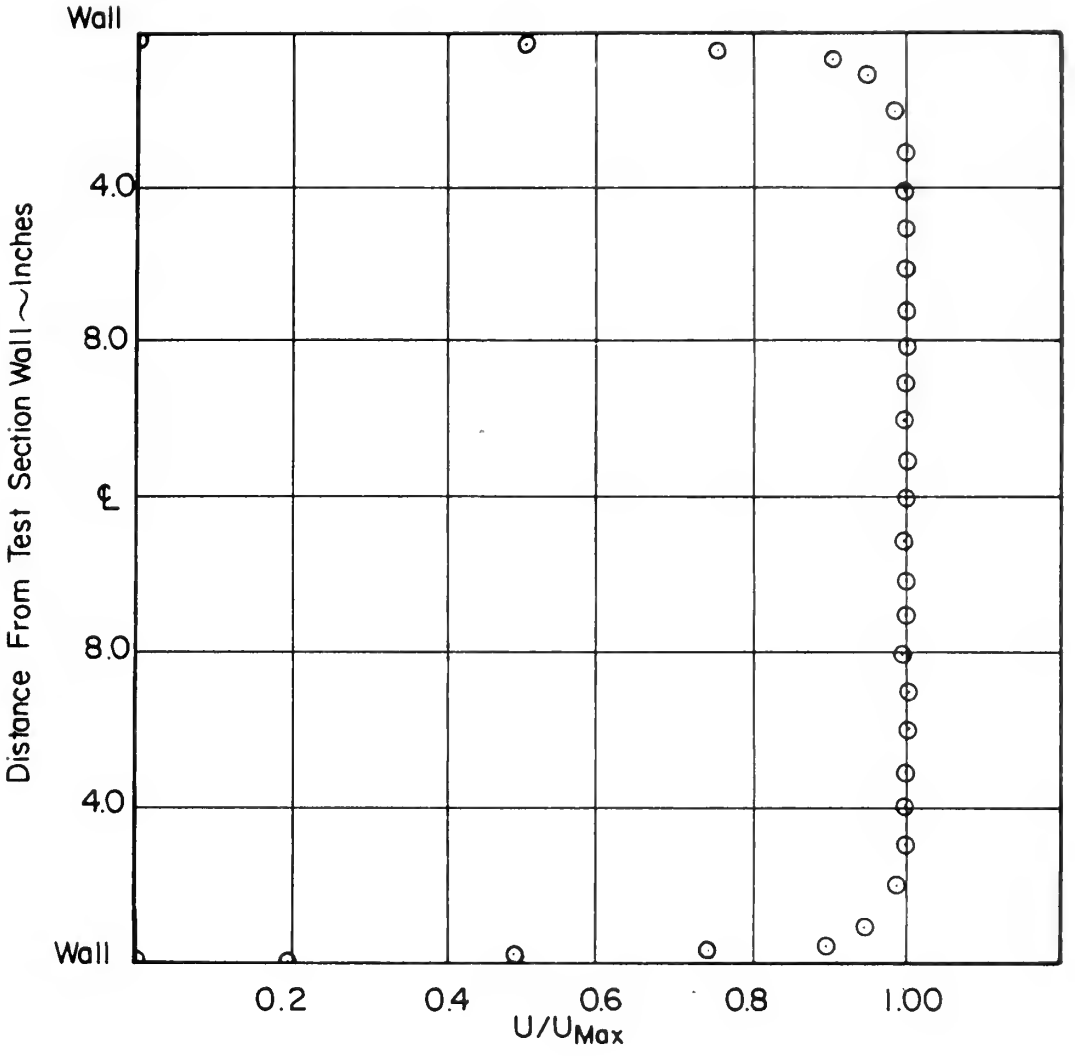

FIGURE 1

TYPICAL WIND TUNNEL TEST SECTION
VELOCITY PROFILE 24 INCHES UPSTREAM
OF MODEL

U_{Max} = 20 ft /sec

FIGURE 2

ROTATING SHUTTER VALVE

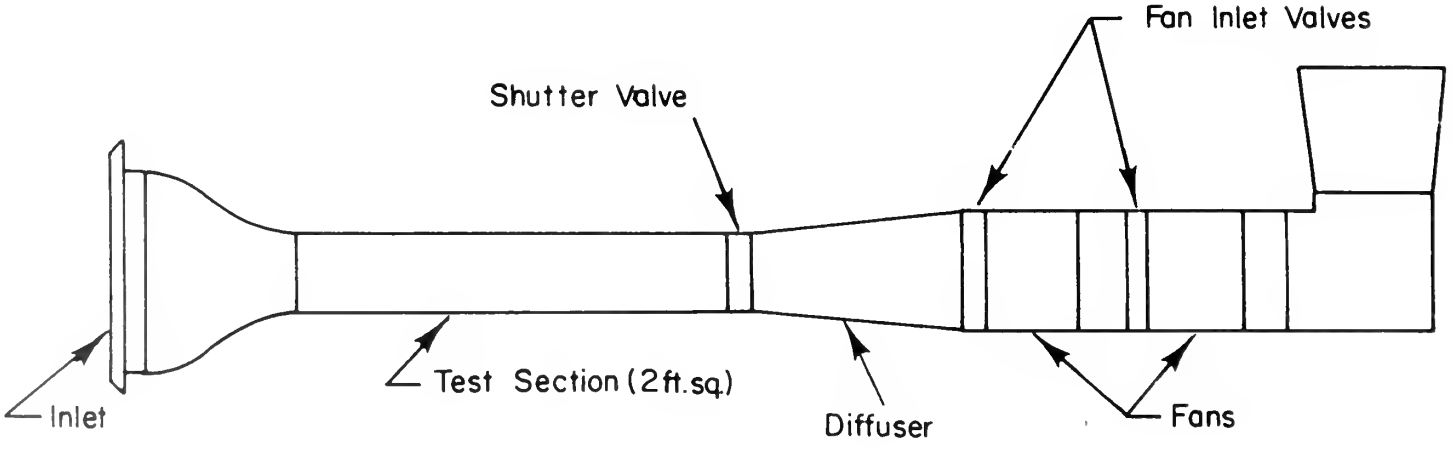

FIGURE 3

PLAN VIEW OF WIND TUNNEL

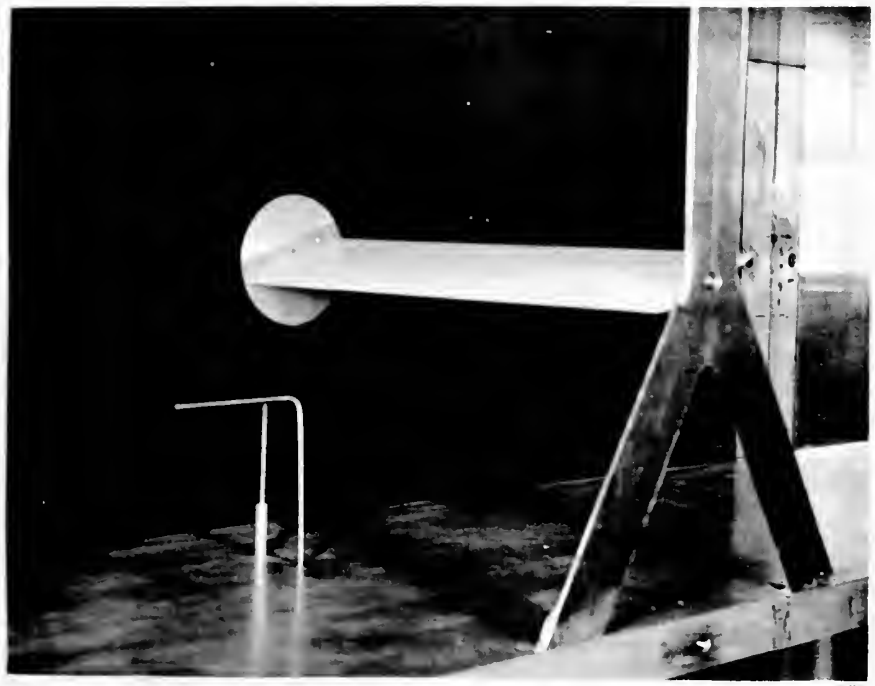

FIGURE 4

WIND TUNNEL MODEL

FIGURE 5

ANGLE OF ATTACK INDICATOR

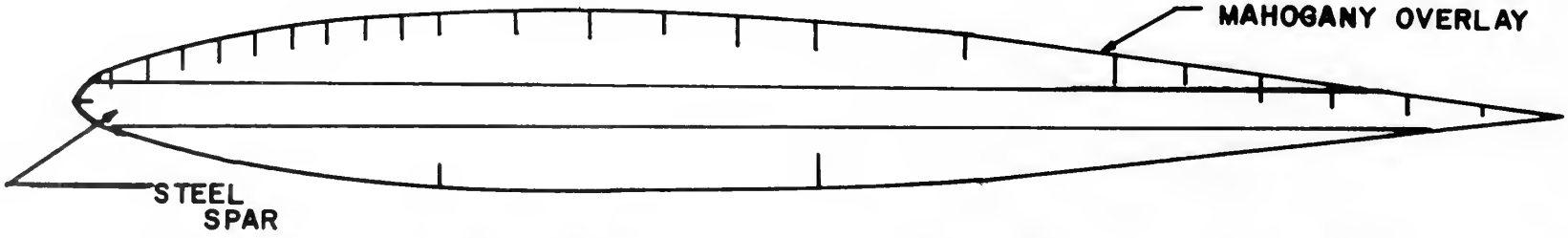

STATION	DISTANCE (X/C)	STATION	DISTANCE
1	.000	13	.350
2	.025	14	.400
3	.050	15	.450
4	.075	16	.500
5	.100	17	.600
6	.125	18	.700
7	.150	19	.750
8	.175	20	.800
9	.200	21	.850
10	.225	22	.900
11	.250	23	.950
12	.300	*24	.250
		*25	.500

* TAPS 24 AND 25 ARE ON LOWER SURFACE

FIGURE 6. PRESSURE TAPS ON WIND TUNNEL MODEL

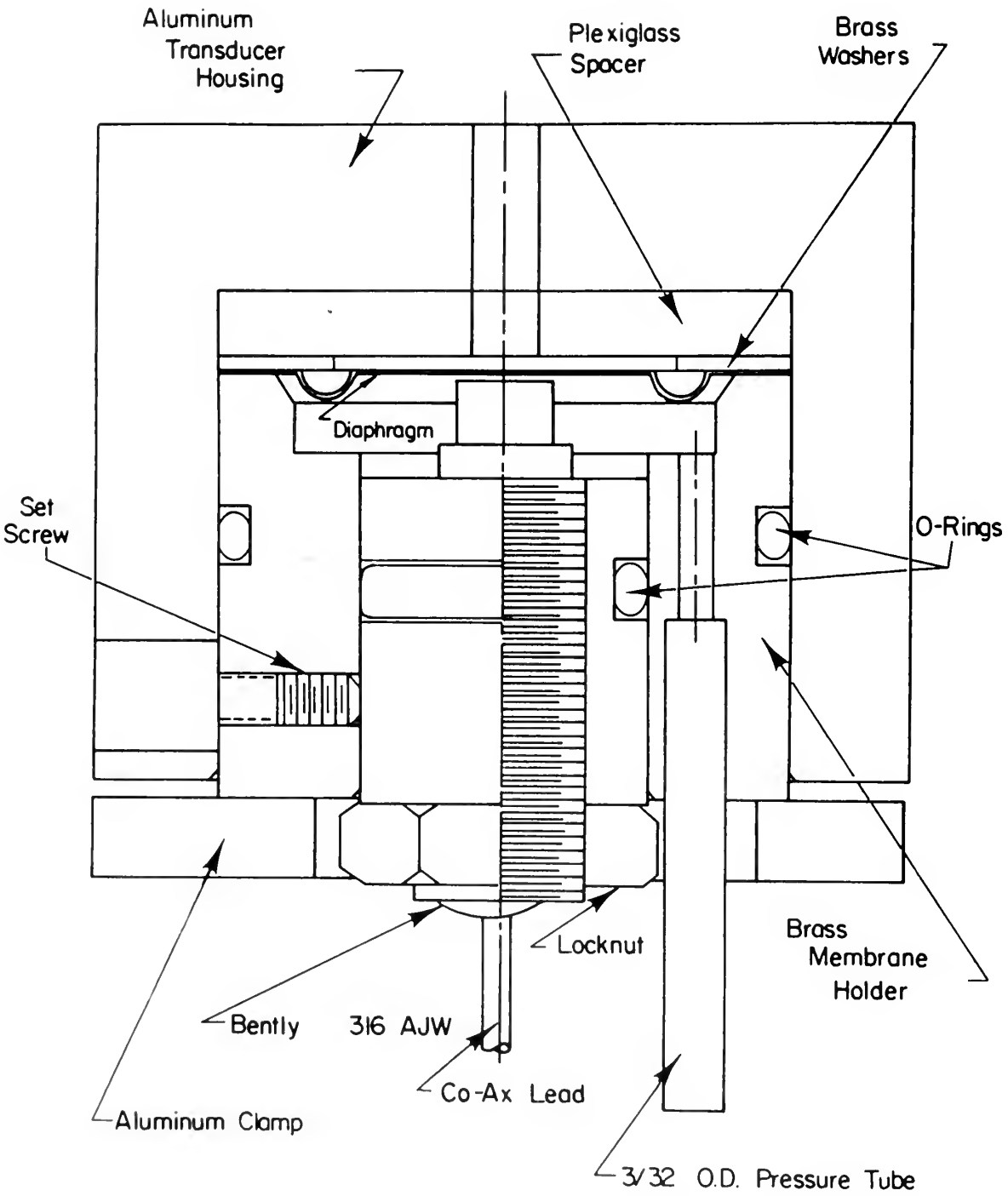

FIGURE 7. SECTIONAL DRAWING OF PRESSURE TRANSDUCER

3. Wind Tunnel Model

The wind tunnel model used was a NACA 63-010 airfoil modified by a straight line fairing from 60% chord aft to the trailing edge to remove the cusp. The model's span was 24 inches with a constant chord of 6 inches. The model was mounted across the test section with a mechanism to allow rotation about the midchord line as is shown in Figure 4. This fixture allowed angle of attack to be varied and measured (see Fig. 5). The model itself was built from a 1/8 inch thick steel spar with wood laminated over it. Twenty-three pressure taps on the upper surface and two on the lower surface were located at midspan (see Fig. 6) and brought through the tunnel walls with stainless steel tubing.

4. Pressure Transducers

A pressure transducer mounted inside the model would have been sensitive to vibrations induced by the unsteady flow. Other limitations on size and expense lead to the selection of remote pressure transducers designed by Prof. L. V. Schmidt. These were similar to ones employed by Johnson [Ref. 6], but with some miniaturization of components and other modifications which made assembly easier. The design is shown in Figure 7. Two transducers were built, one to measure pressures on the model and the other to be used as a reference.

The transducer system consisted basically of a Bentley Detector System, a 0.003 inch thick annealed brass diaphragm mounted in an aluminum housing, and plastic and steel tubing

enabling the pressure on the airfoil to be transmitted to the transducer diaphragm cavity. The diaphragm thickness was selected so as to provide a usable pressure sensing instrument in the pressure range of ± 0.75 psia. The assembled transducer is shown in Figure 8.

The Bentley Detector System provides a voltage signal which is linear with respect to the distance change detected by its probe. For small pressure differentials across the brass diaphragm, its deflection is proportional to the pressure. The probe detects deflection of the diaphragm and the output from the distance detector is proportional to this distance. By putting a known pressure differential across the diaphragm, the transducer can be calibrated yielding a linear calibration curve for small differentials. The results of the static calibration are given in Figure 9 and the procedure discussed in Appendix A.

The stainless steel and plastic tubing act as transmitting lines from the pressure taps to the transducer. The unsteady pressure components undergo frequency-dependent phase shift and attenuation through the tubing. A dynamic calibration (Appendix A) was performed and the results may be seen in Figures 10 and 11.

5. Miscellaneous Instrumentation

The distance detector system was initially calibrated using a digital voltmeter and a True Root Mean Square Meter. For static calibration, the signal from the distance detector and a bias voltage were put through a D.C. amplifier and the output read on the digital voltmeter.

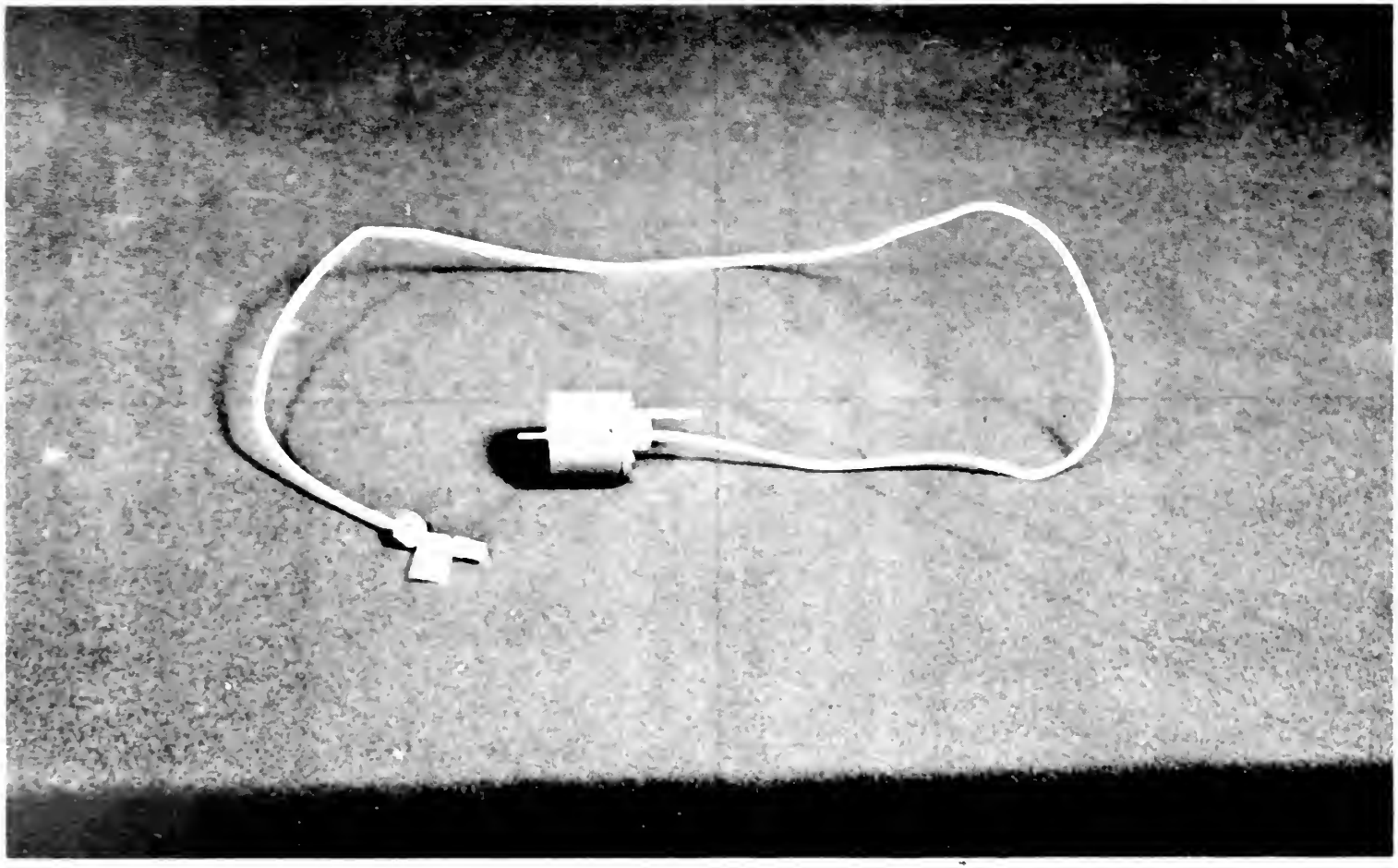

FIGURE 8. ASSEMBLED TRANSDUCER

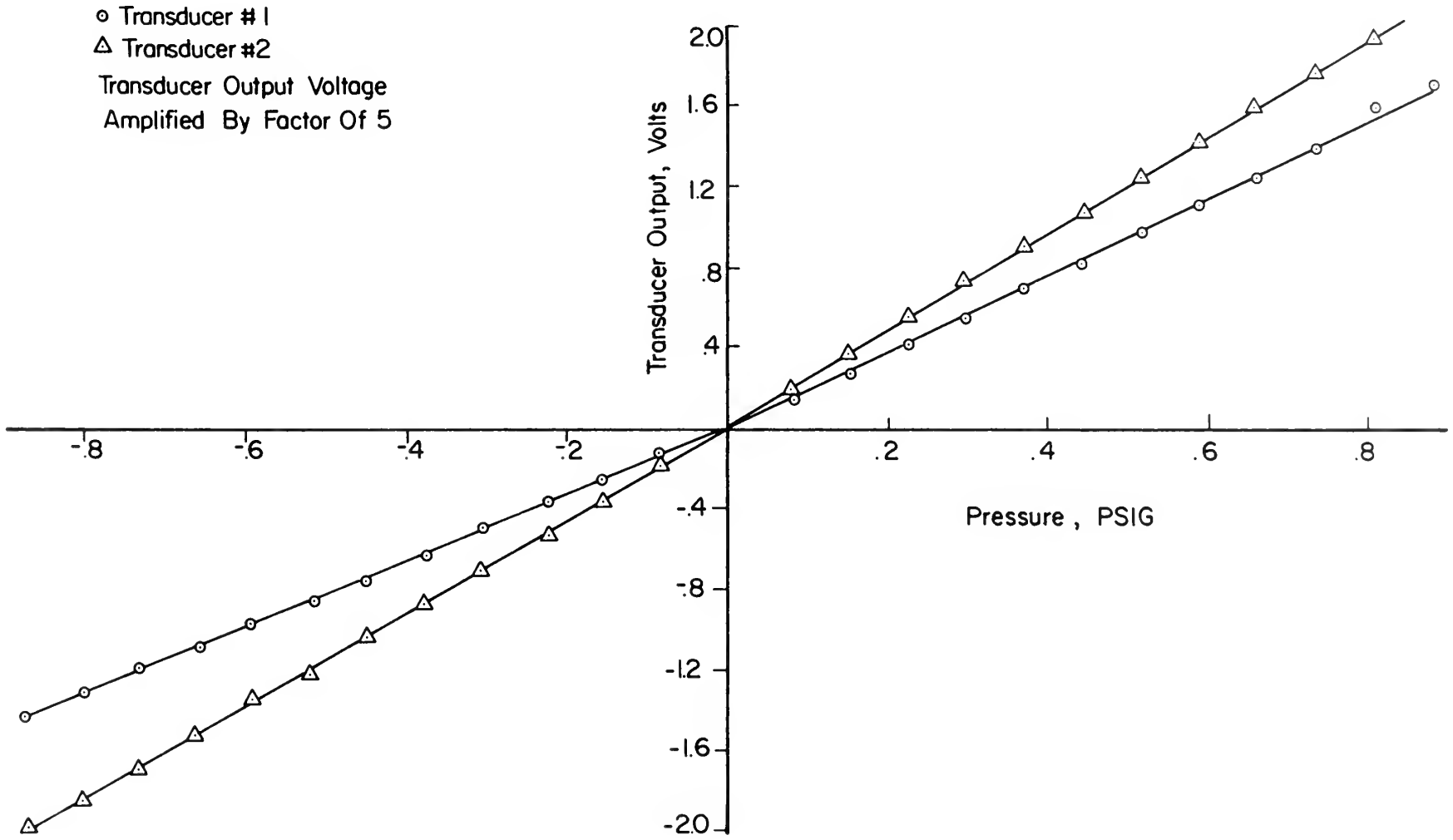

FIGURE 9. PRESSURE TRANSDUCER STATIC CALIBRATION CURVE

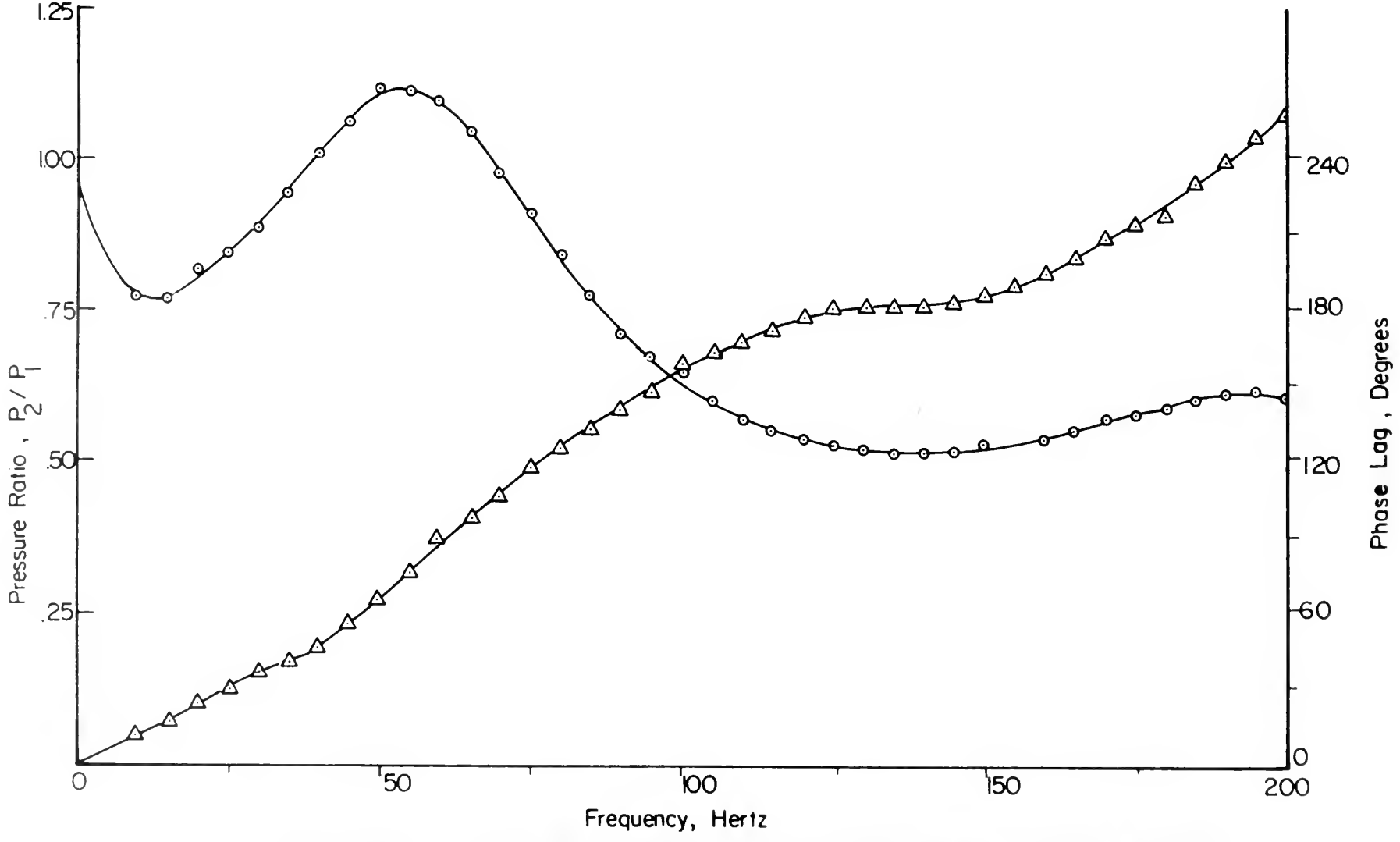

FIGURE 10 DYNAMIC RESPONSE OF PRESSURE TRANSDUCER #1

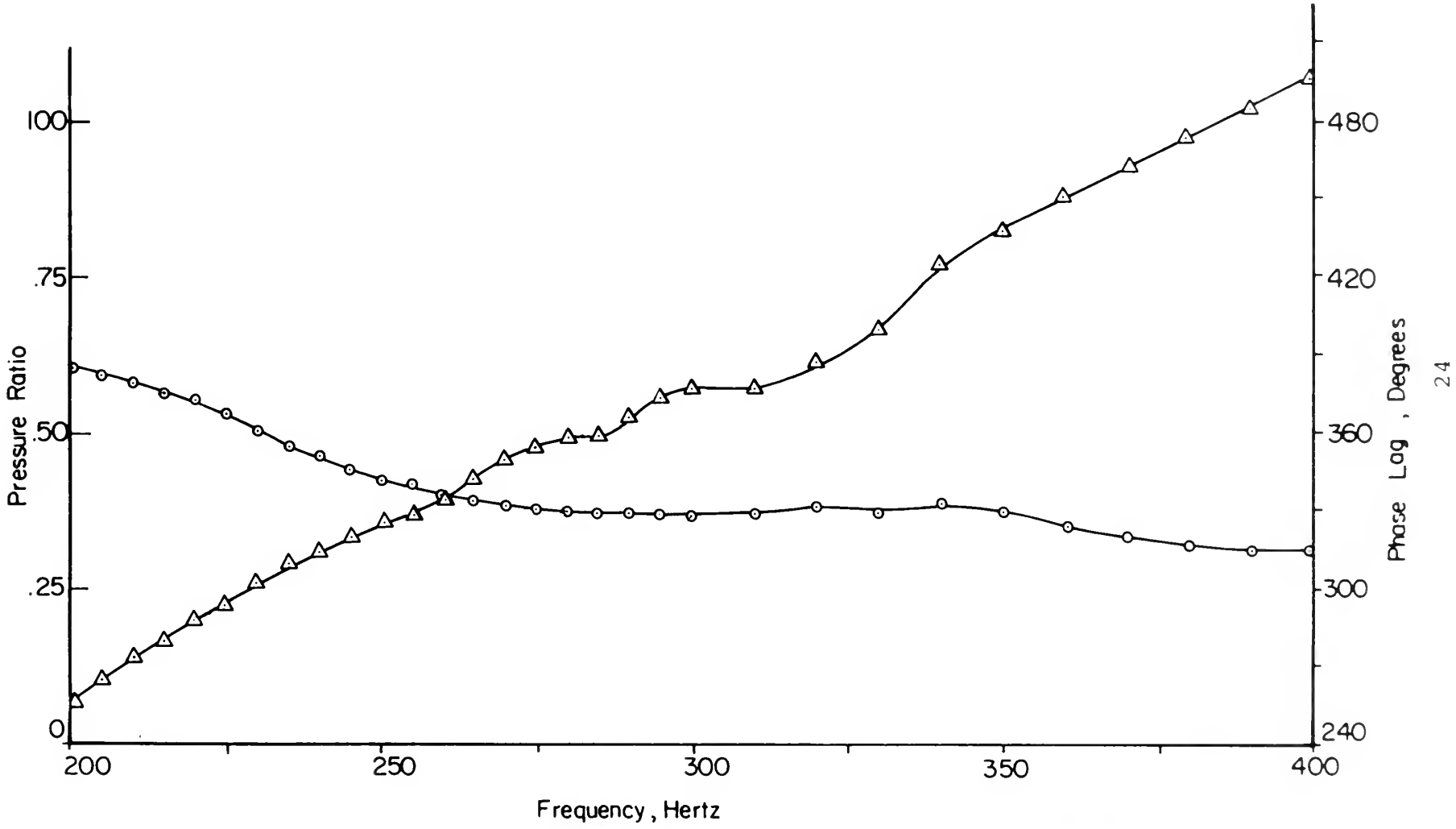

FIGURE 11 DYNAMIC RESPONSE OF PRESSURE TRANSDUCER #1

An acoustical driver unit provided the unsteady pressure input for dynamic calibration. This unit was driven by the voltage signal from a wide range audio oscillator which was amplified by a power amplifier. Phase readings were obtained using a precision phase meter and checked visually on a dual-beam oscilloscope. The schematics of the system used for the dynamic calibrations are shown in Figures 12, 13, and 14.

The mean dynamic pressure in the oscillating wind tunnel was read from a micromanometer connected to a pitot-static tube. The oscillating component of the free-stream velocity was measured using a constant temperature, transistorized, hot-wire-anemometer probe. Figures 15 and 16 give typical calibration results of the hot wire showing linear voltage output with velocity and a Blasius Profile measurement.

A magnetic pickup located outboard of the upper shutter blade shaft was used to measure shutter valve frequency. This output was read on a decade counter and used to trigger the dual-beam oscilloscope. A wave analyzer was used to measure the Fourier components of the velocity. Velocity and pressure outputs were recorded photographically from the oscilloscope. The hot wire anemometer inverted the signal from the hot wire, such that all photographs show the velocity waveform inverted. The instrumentation system is shown schematically in Figure 17 and pictorially in Figure 18.

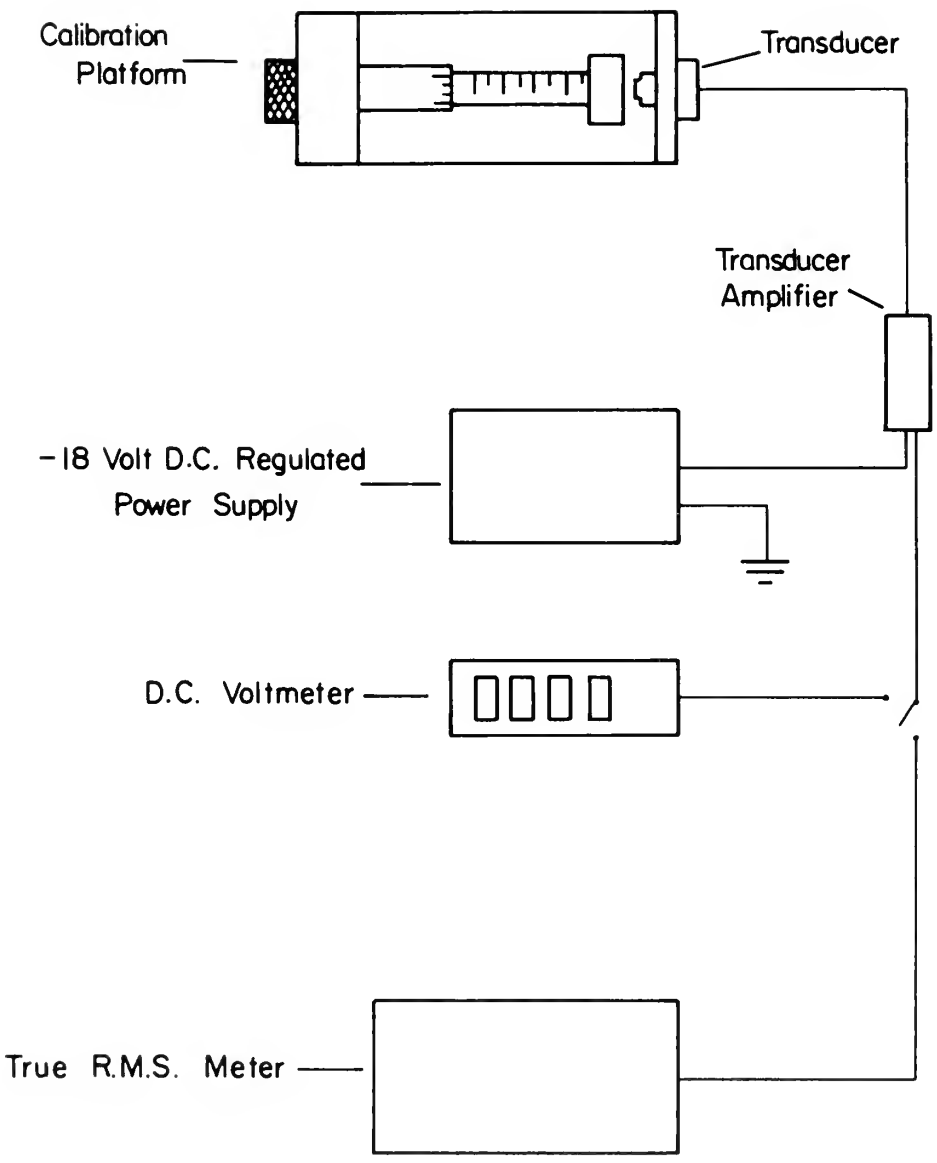

FIGURE 12. PROXIMITY DETECTOR CALIBRATION INSTRUMENTATION

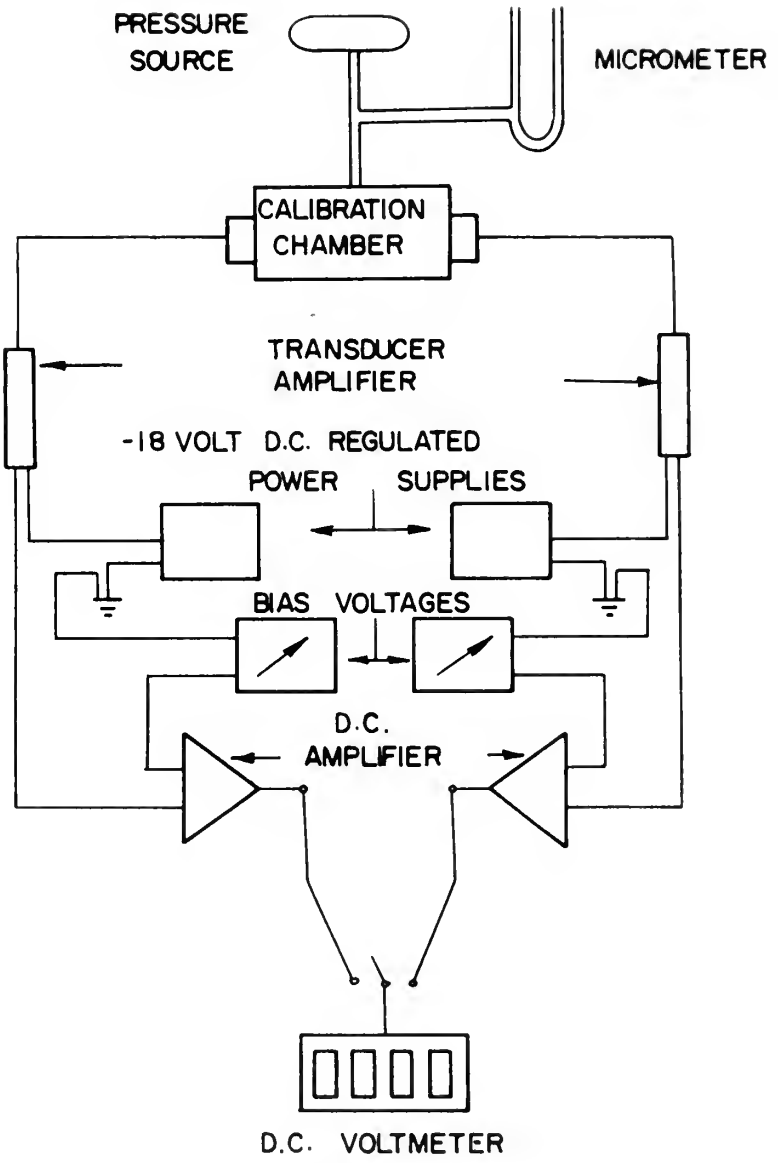

FIGURE 13 STATIC CALIBRATION INSTRUMENTATION

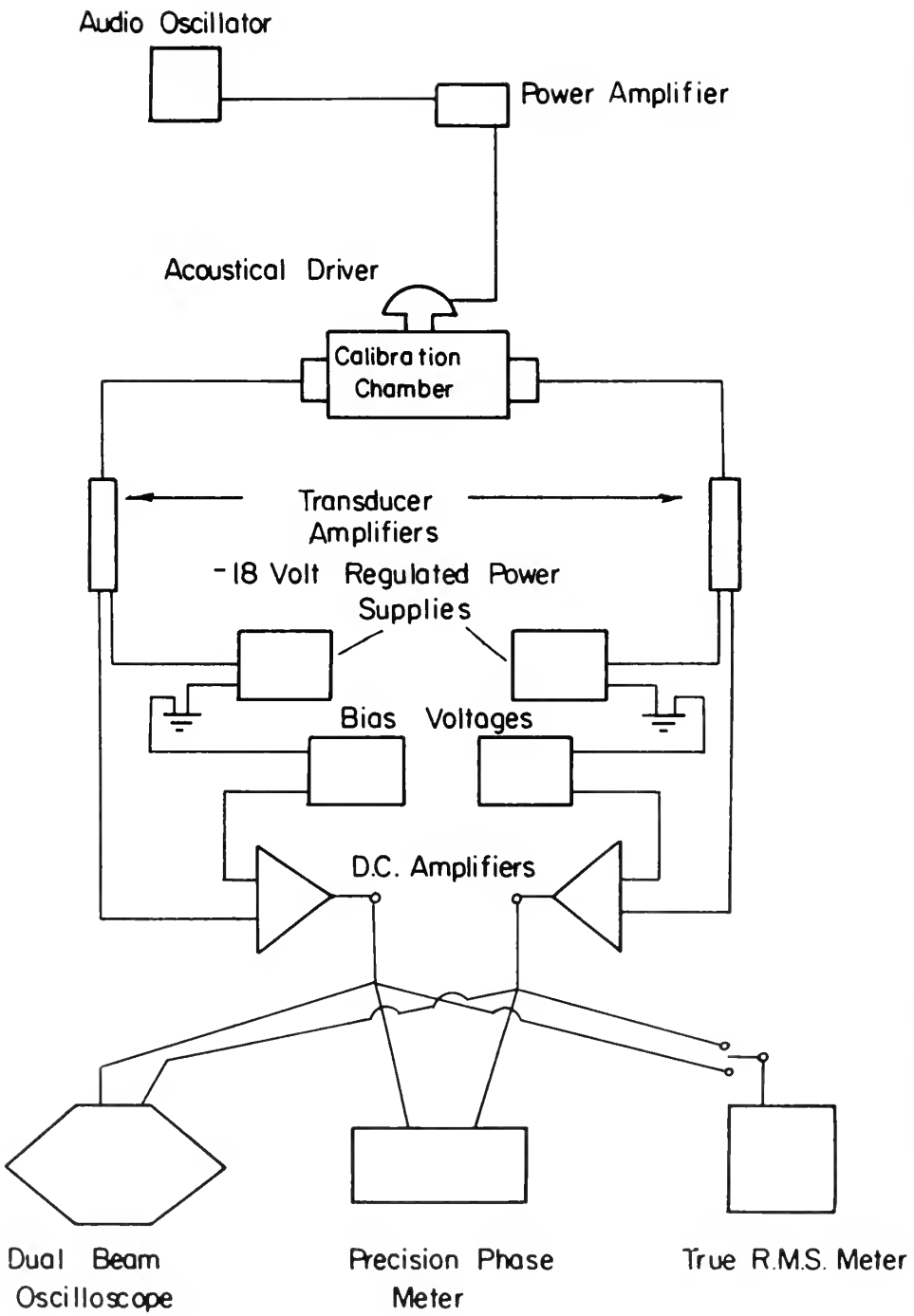

FIGURE 14. DYNAMIC CALIBRATION INSTRUMENTATION

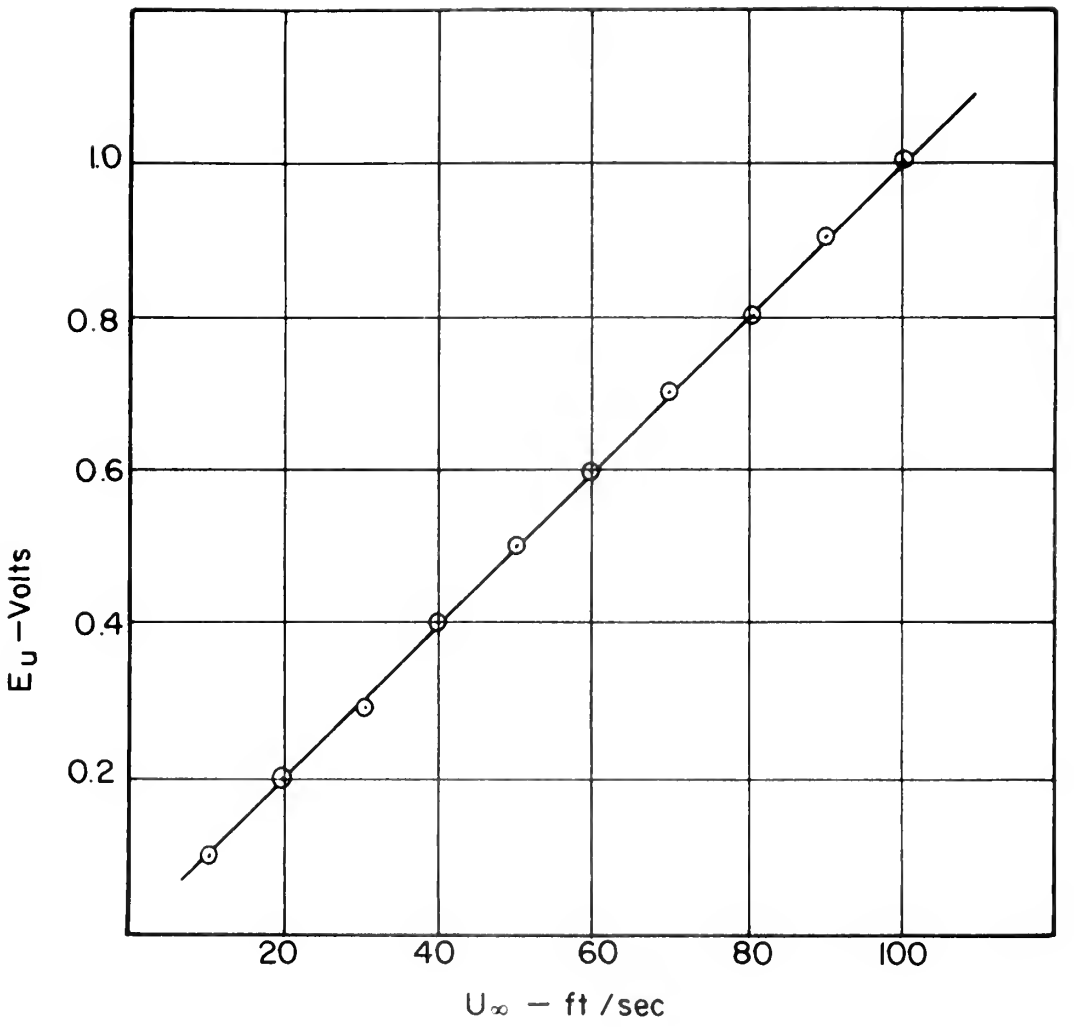

FIGURE 15

TYPICAL HOT WIRE ANEMOMETER CALIBRATION CURVE
(STEADY FLOW)

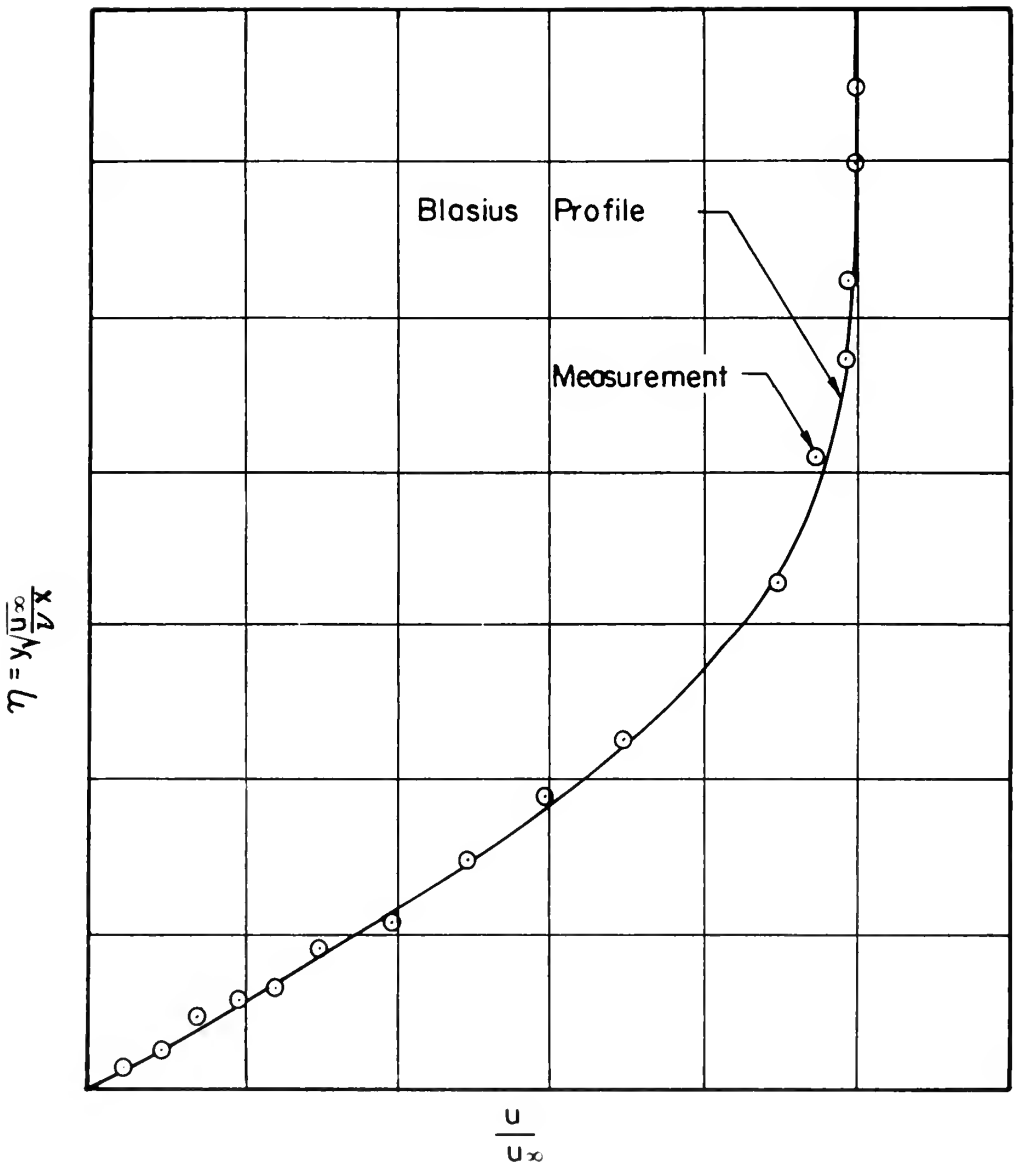

FIGURE 16

TYPICAL HOT WIRE ANEMOMETER CALIBRATION
VELOCITY PROFILE IN BLASIUS
FLOW

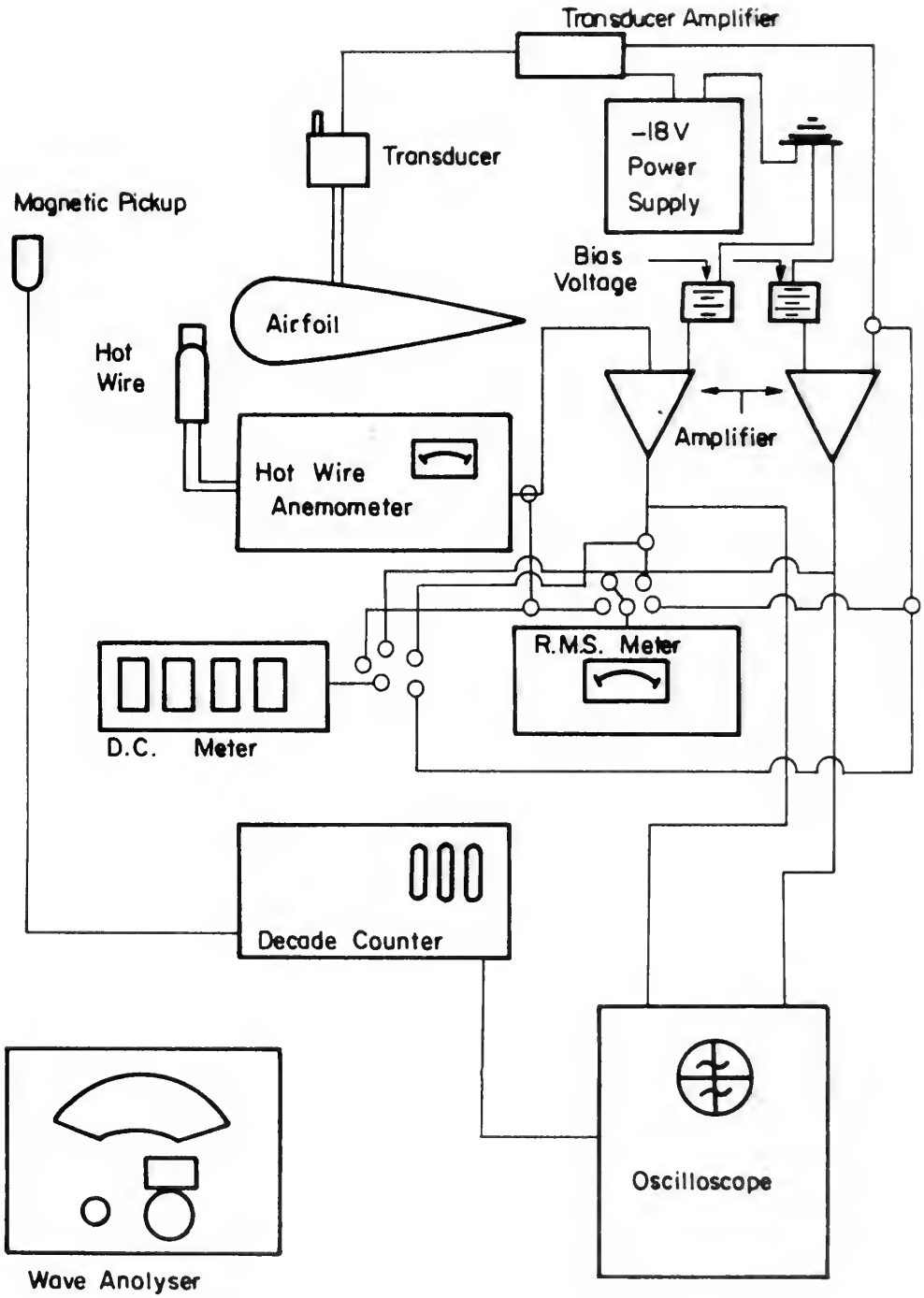

FIGURE 17

WIND TUNNEL INSTRUMENTATION

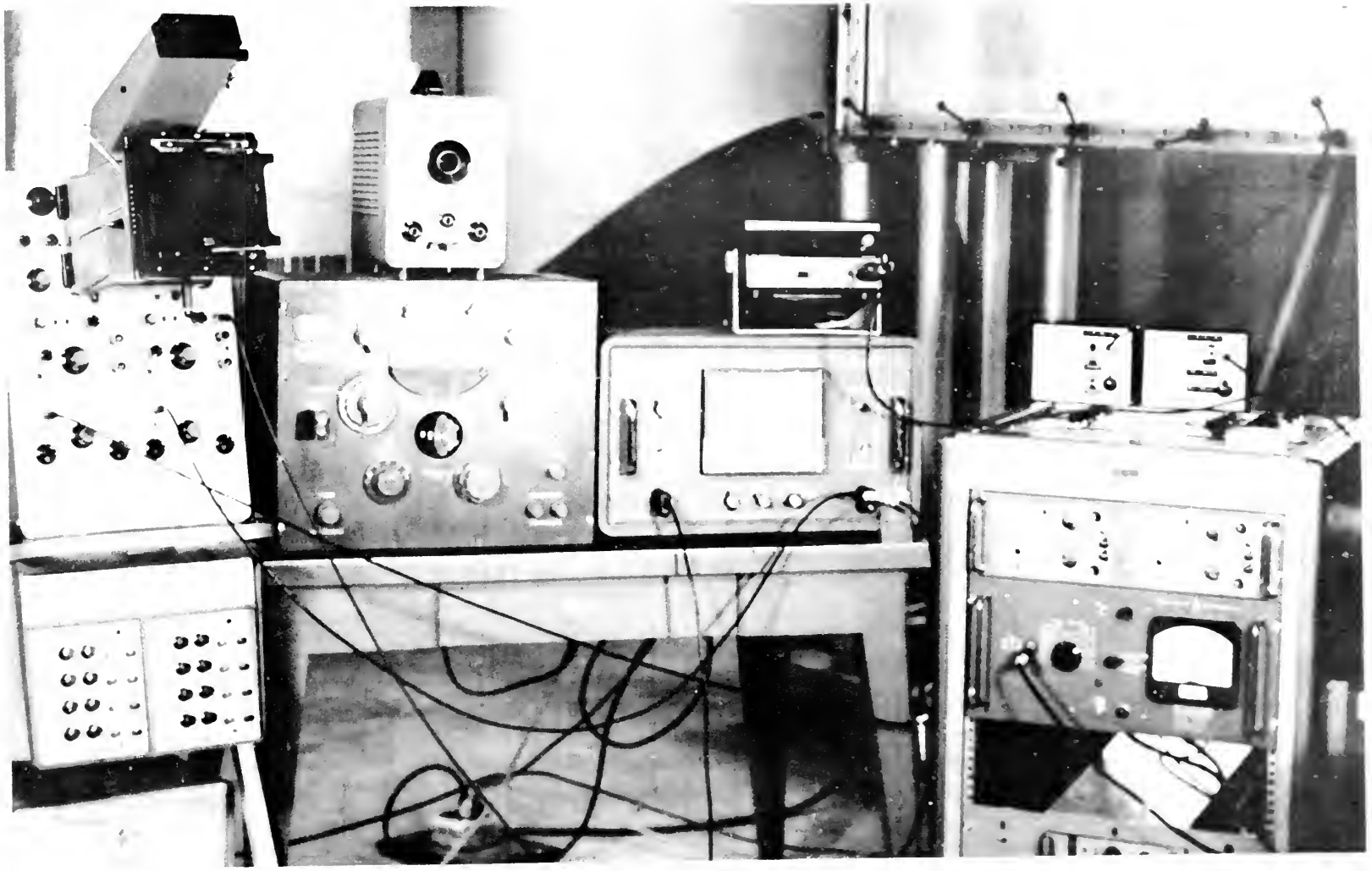

FIGURE 18. WIND TUNNEL INSTRUMENTATION

III. WIND TUNNEL PROCEDURE

After the model had been installed in the tunnel, the pressure transducer was set up near the steel tubing protruding from the model and was isolated from the tunnel vibrations. A styrofoam box was used to enclose the transducer and to reduce thermal drift.

Because of the "organ pipe effect" of the tunnel, there were only two or three frequencies at each selected mean velocity in which the free-stream velocity waveform was relatively free of higher frequency components and almost purely sinusoidal. For the purposes of this work, a high Reynolds number was desirable. A mean freestream velocity of one hundred feet per second was obtained using 4-inch blades. Frequencies that gave clean waveforms at this speed were 94, 128, and 154 hertz. Unfortunately time limitations made it possible to investigate only the first two frequencies.

Initially zero angle of incidence was located. This was done by comparing the two pressure taps on the lower surface with the two corresponding taps on the upper surface. Angle of attack adjustments were made until the readings were identical on both surfaces. It was found that the angle of attack vernier was accurate with $\pm$ 0.05 degrees.

The D.C. amplifiers used in this work introduced phase shifts in the input signals. In order to measure relative phase shifts between velocity and pressure, the hot wire output was also processed by one of these amplifiers. It was

previously determined that the two amplifiers did have identical phase shift characteristics. This was done by putting the same input into both amplifiers and observing zero phase shift between their outputs.

In order to insure that the oscillating free stream velocity was relatively free of higher harmonics, the hot wire output was manually scanned by the wave analyzer. When the amplitude of the second harmonic was less than 8% of the first, the velocity waveform was deemed acceptable.

When all initial set-ups had been completed, runs were made at both frequencies at 0, 10, and 20-degree angles of attack. D.C. voltages were read before the amplifier and R.M.S. voltages after amplification. The relative phase shift between free-stream velocity and the pressure signal was recorded. A steady-flow run was also made at the three angles of attack and the D.C. voltage read.

A photographic record for each of the unsteady flows was made at selected pressure ports. It was unnecessary to take pictures of the outputs at all of the taps, since changes between adjacent taps were too small to be observed visually.

Since the airfoil was symmetrical, measurements for the positive angle of attack were taken from the upper surface at positive angle of attack. Then the airfoil was rotated to a negative angle of attack, the measurements from the same taps taken again, and these were assumed to be the same that the lower surface would have had at a positive angle of attack. The two taps on the lower surface provided a check on the validity of this procedure.

IV. RESULTS AND DISCUSSION

Measurements were taken at each pressure tap to determine the phase shift of the pressure waveform in relation to the velocity waveform. The precision phase meter used was only valid for measuring phase shifts between identical waveforms. At 128 hertz, the pressure and velocity waveforms were similar and meaningful phase readings could be made. The results are summarized in Table I and plotted in Figure 19 for zero angle of attack. However, at 94 hertz, higher harmonics distorted the pressure waveform so that only phase shift readings of questionable validity could be taken. (See Figure 20).

Figures 20-24 show typical oscilloscope traces of the velocity and pressure waveforms at selected pressure taps. The velocity waveforms, it should be recalled, are inverted. From these photographs, it may be seen that secondary and higher harmonics appear very distinctly at 94 hertz at all three angles of attack, but are not noticeable at 128 hertz. This is probably due to the fact that the pressure transducer tends to act as a filter. Referring back to Figures 10 and 11, second-order harmonics of the fundamental pressure frequencies were attenuated by 0.3 for 256 hertz and by .6 for 188 hertz. Thus, second-order harmonics would be negligible at the higher frequency.

It was noted the higher harmonics in the pressure waveforms seem to be increasingly reduced going chordwise from

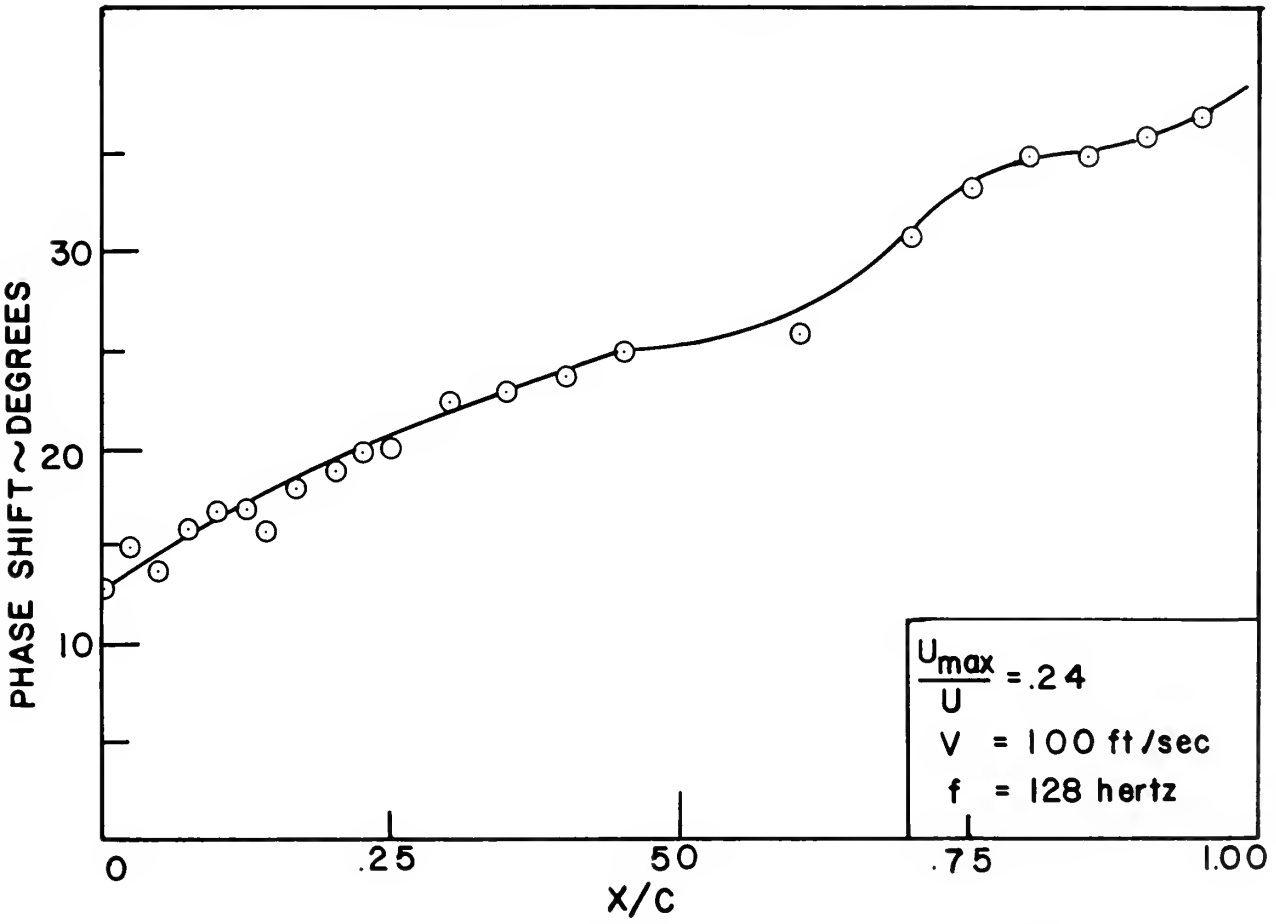

FIGURE 19. PHASE SHIFT vs. DISTANCE ALONG CHORD
$\alpha = 0°$

Velocity-10 volts/cm.

Tap #1

Pressure-2 volts/cm.

Tap #5

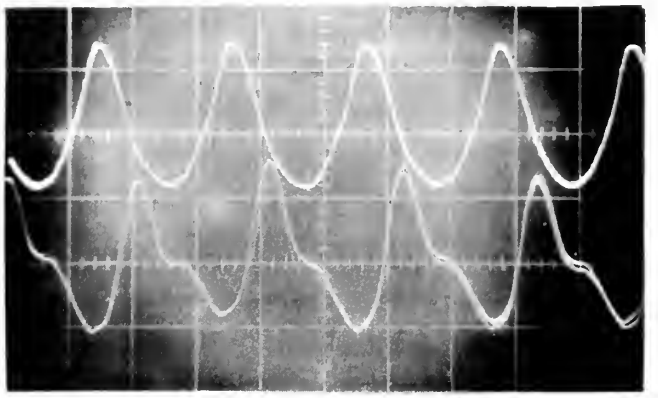

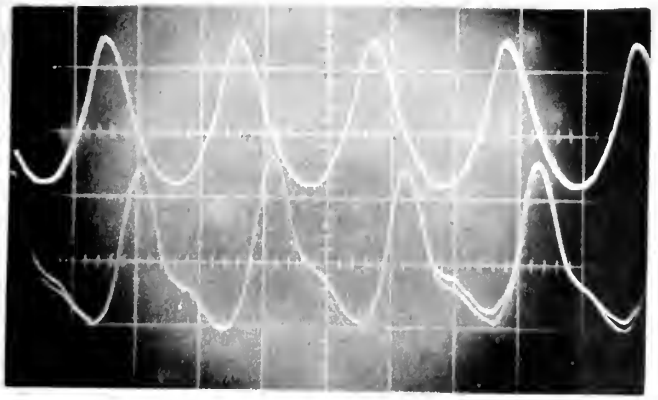

Tap #15

FIGURE 20

PRESSURE AND VELOCITY WAVEFORMS

$f = 94$ hertz

$\alpha = 0$ degrees

Tap #23

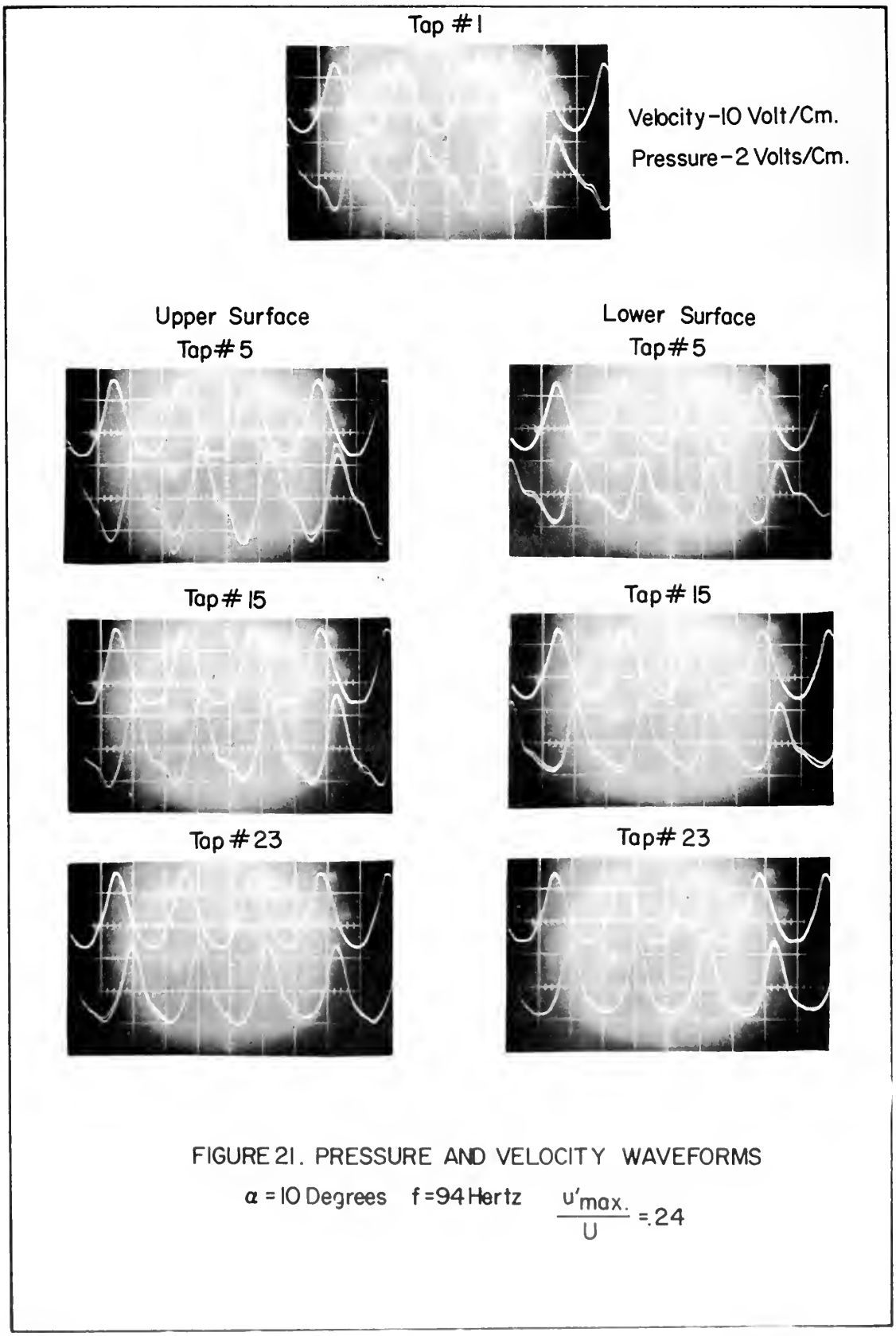

FIGURE 21. PRESSURE AND VELOCITY WAVEFORMS

α = 10 Degrees f = 94 Hertz $\frac{u'_{max.}}{U}$ = .24

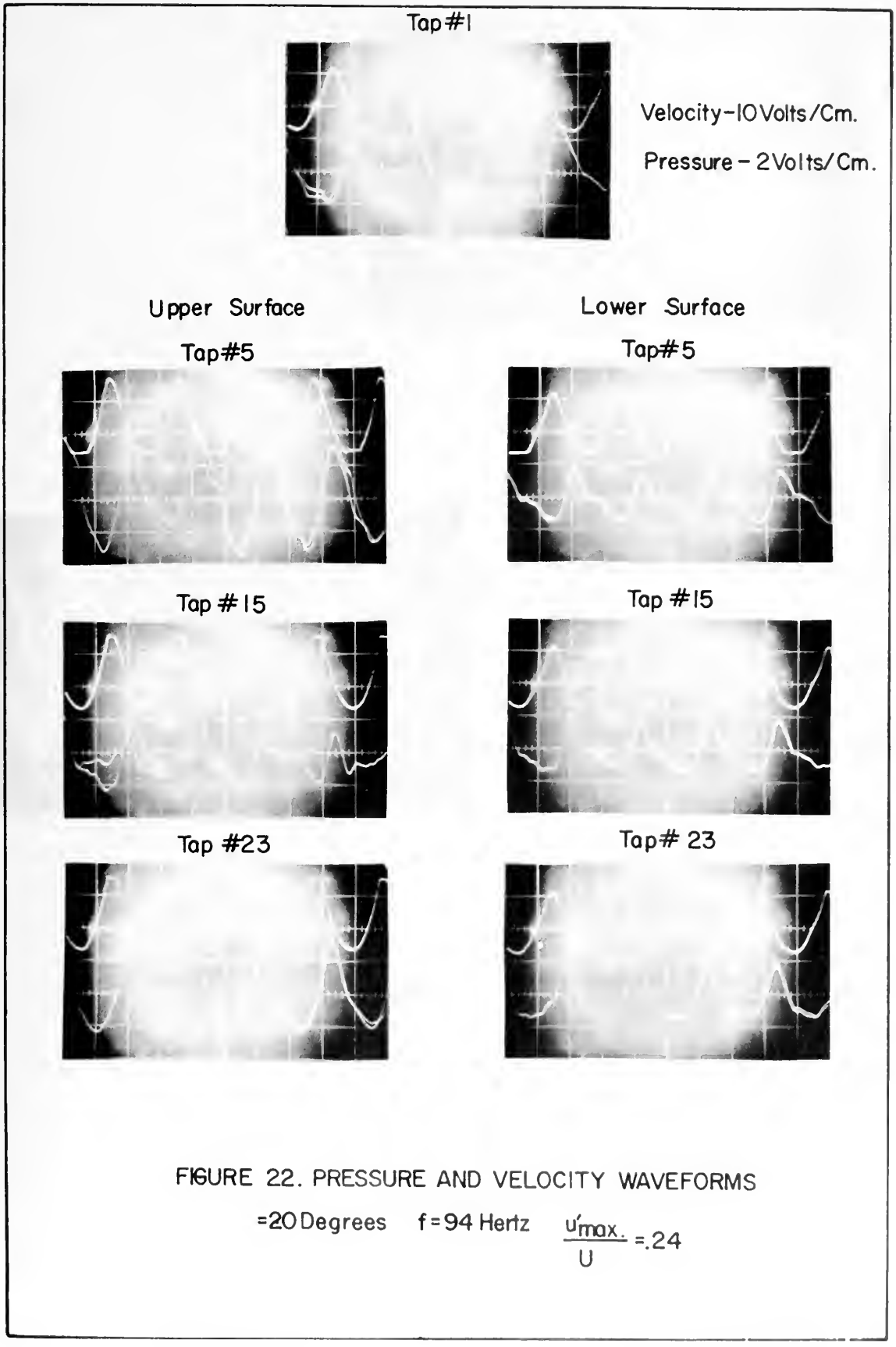

FIGURE 22. PRESSURE AND VELOCITY WAVEFORMS

=20 Degrees f=94 Hertz $\frac{u'_{max.}}{U}$ =.24

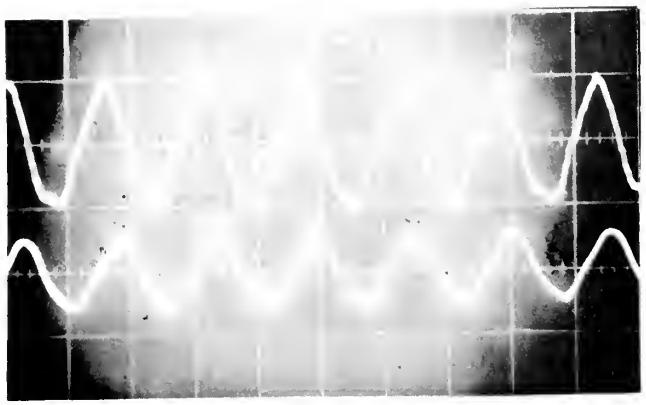

Velocity-5 volts/cm.

Tap #1

Pressure-5 volts/cm.

Tap #18

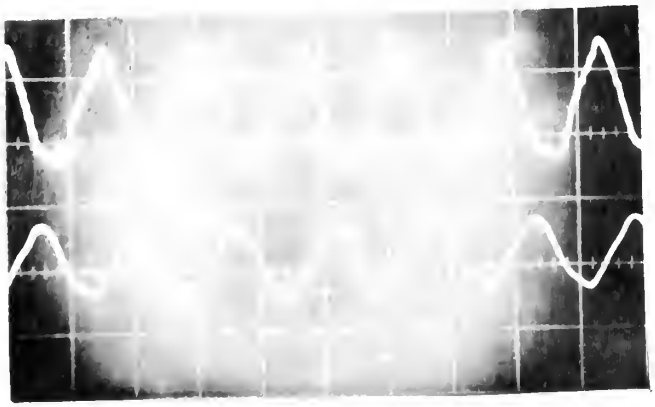

Tap #23

FIGURE 23. VELOCITY AND PRESSURE WAVEFORMS
f = 128 hertz α = 0 degrees

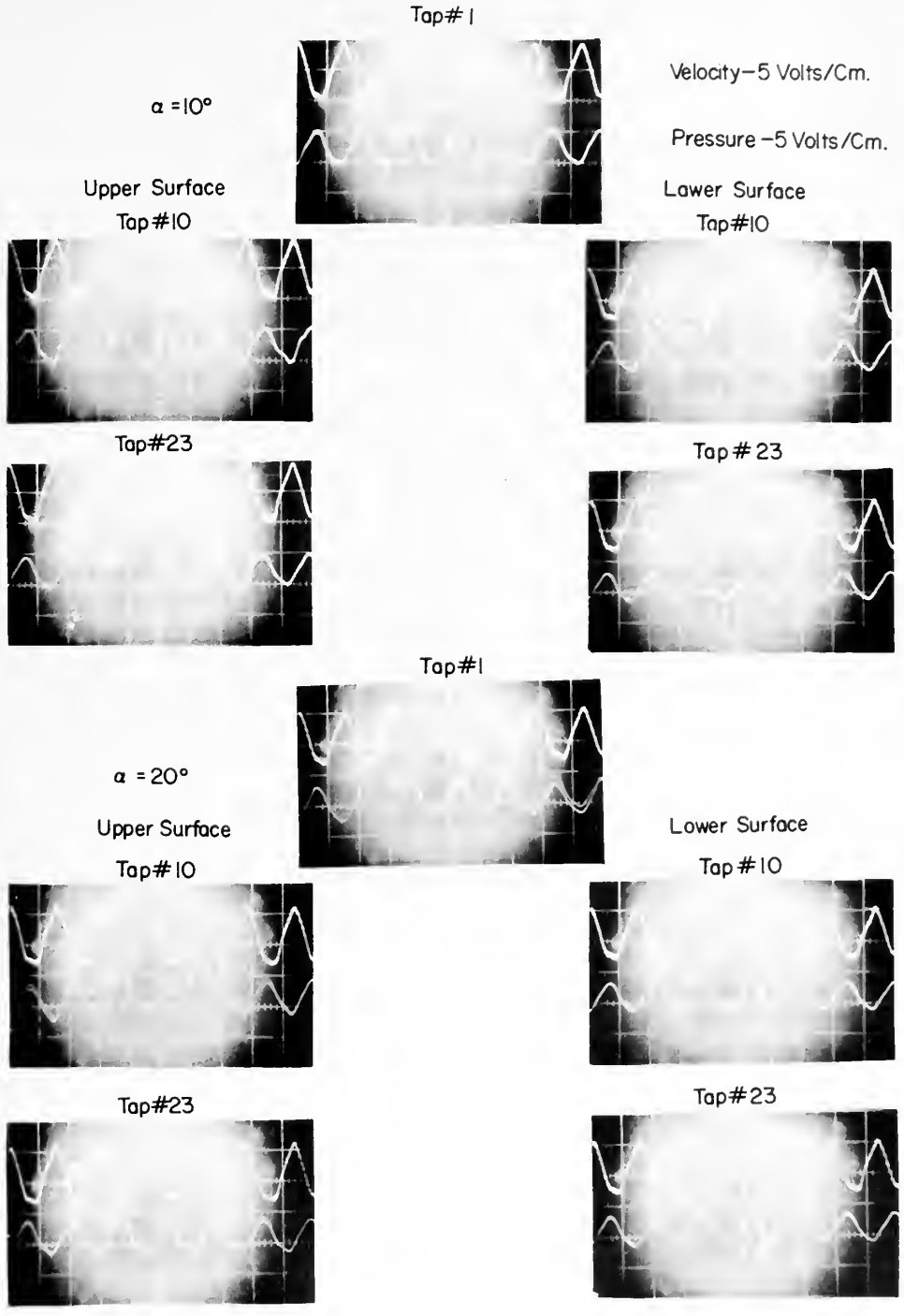

FIGURE 24. PRESSURE AND VELOCITY WAVEFORMS

$\frac{u'_{max.}}{U} = .10$ f =128 Hertz

the leading edge to the trailing edge. The sequence of photographs in Figure 21 are typical.

Waveforms of varying amplitude and shape superimposed on each other may be seen in some of the oscilloscope photographs. These are indicative of separation and its associated turbulence. An example of this is shown in Figure 22 at tap 1. Looking at tap 23 on the upper surface, in the same figure, the effects of separation seem to be less radical. Two theories have been formulated to explain this.

One was suggested to the author by Despard [Ref. 8]. An early transition to a turbulent boundary layer occurs as a result of oscillating flow. Early transition causes the separation point to be moved downstream. As separation begins, vortices are shed. These are large enough to effect the pressure transducer; however, moving back from the point of separation, the individual vortices break down in the wake. Thus, as the trailing edge is neared, the vortices lose their strength and the transducer feels only the free stream pressure impressed upon it. A sketch of such a flow field is shown in Figure 25.

A second explanation is that the flow becomes fully detached at the leading edge, but then re-attaches at some point downstream.

Both theories are plausible, due to the fact that the normal force coefficient, C_n, was greatly increased in oscillating flow as compared to steady flow for α = 10 and 20 degrees. Either early transition or reattachment would cause

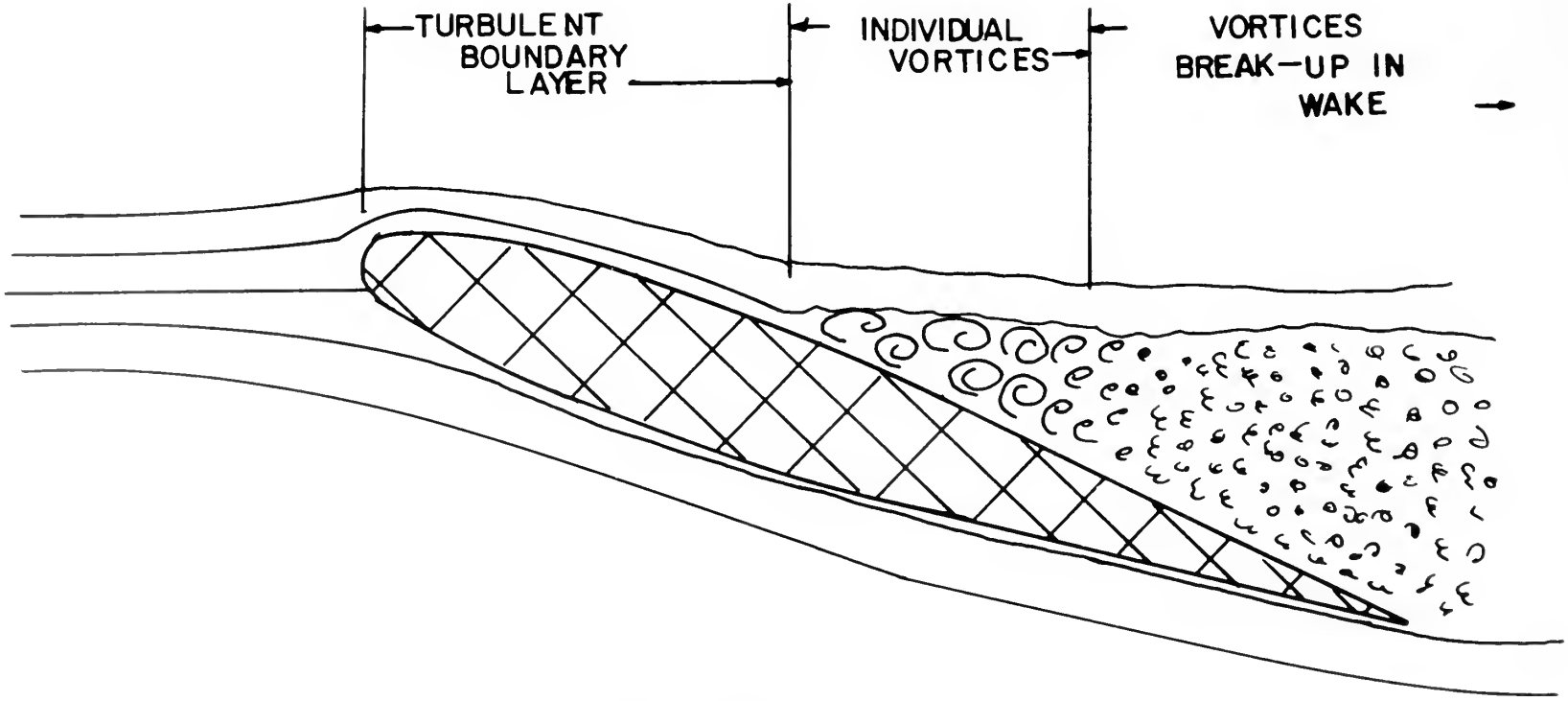

FIGURE 25
SEPARATED FLOW IN OSCILLATING FREESTREAM

an increase in lift. In an attempt to resolve this question a steady flow run was made at α = 10 degrees with a 1/16 inch wire fastened the length of the span just aft of the leading edge in order to trip the boundary layer into early transition. There was no appreciable increase in lift.

The normal force coefficient was found from:

$$C_n = \oint C_p d(x/c) \quad .$$

These values are plotted in Figure 26. The mean pressure coefficients for each frequency and each angle of attack were calculated. These are summarized in Table II and plotted in Figures 27 through 33. Since the pressure transducer measured the pressure differential between local static pressure and atmospheric pressure, it made the following definition of C_p very convenient:

$$C_p = \frac{P_{sl} - P_{atm}}{q} \quad .$$

Since stagnation pressure is equal to atmospheric pressure,

$$C_{pstag} = 0.00 \quad .$$

In Figure 27, it may be seen that the mean pressure distribution is not dependent on frequency for zero angle of attack.

The root mean square of the pressure was converted to the nondimensional C_p':

$$C_p' = \frac{P_{rms} - P_a}{q} \quad .$$

These values are tabulated in Table III and a distribution for α = 20°, f = 128 hertz, plotted in Figure 34. In general,

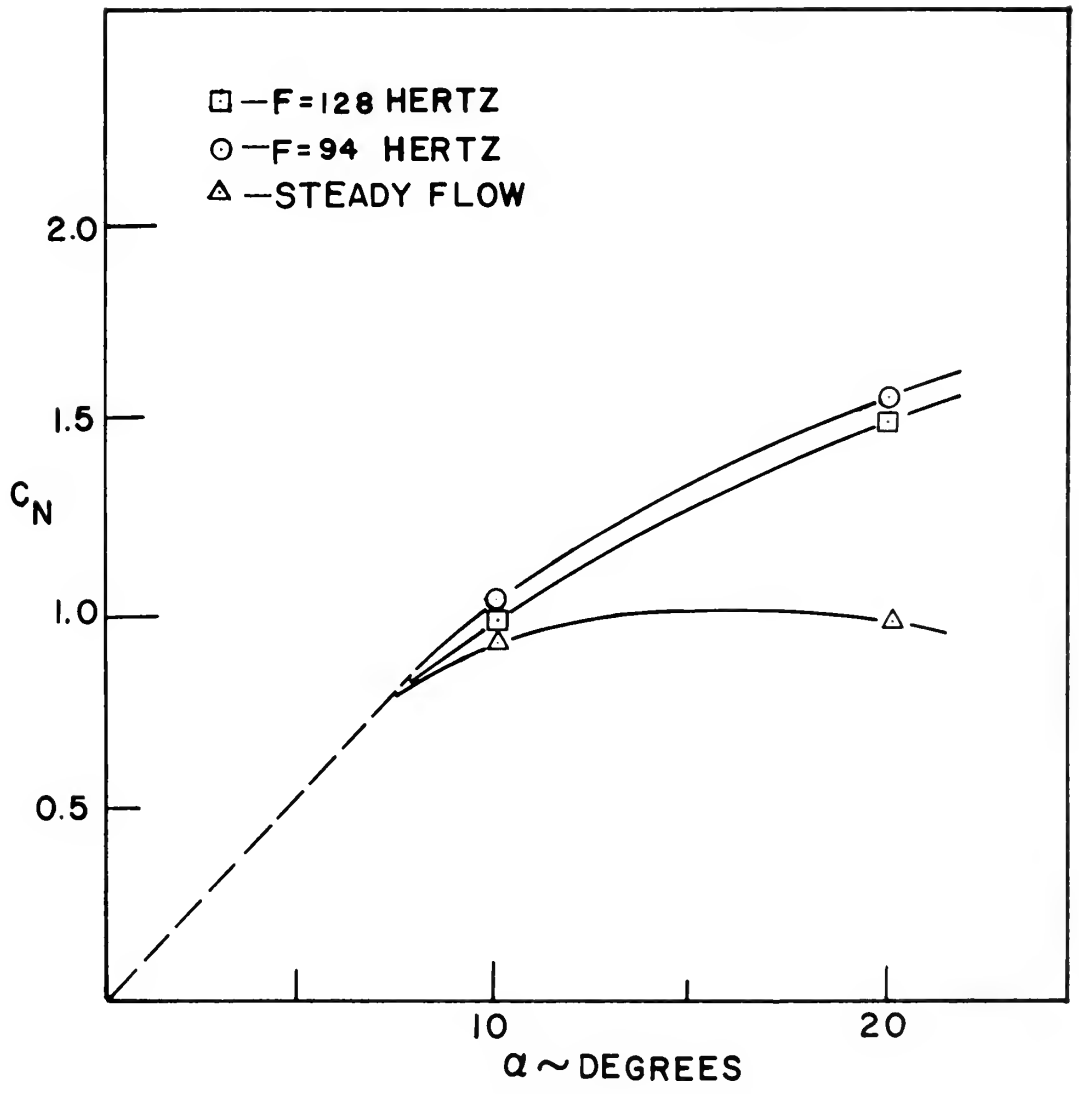

FIGURE 26. C_N vs. α

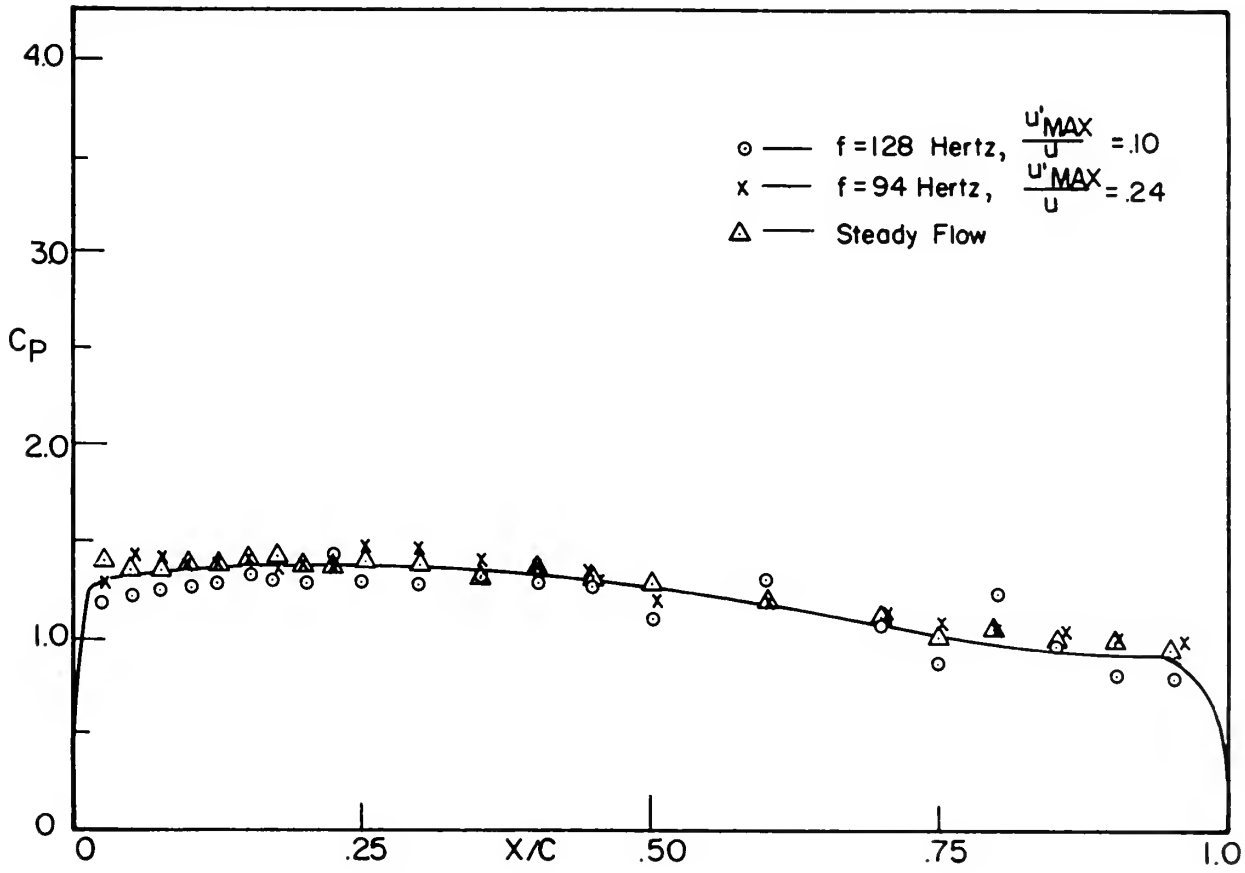

FIGURE 27

MEAN PRESSURE DISTRIBUTION ON AIRFOIL

$\alpha = 0°$ V = 100 ft/sec

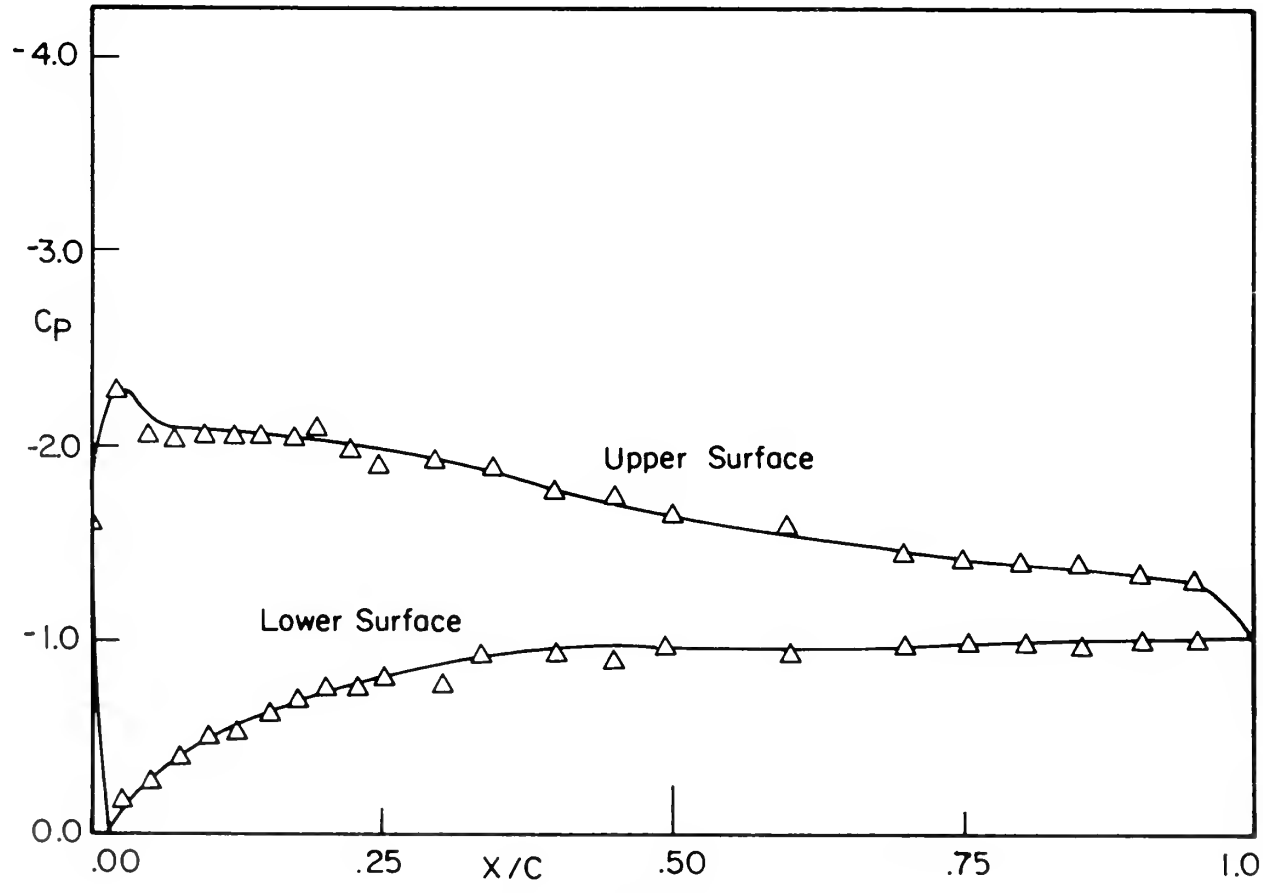

FIGURE 28

MEAN PRESSURE DISTRIBUTION ON AIRFOIL

$\alpha = 10°$ STEADY FLOW

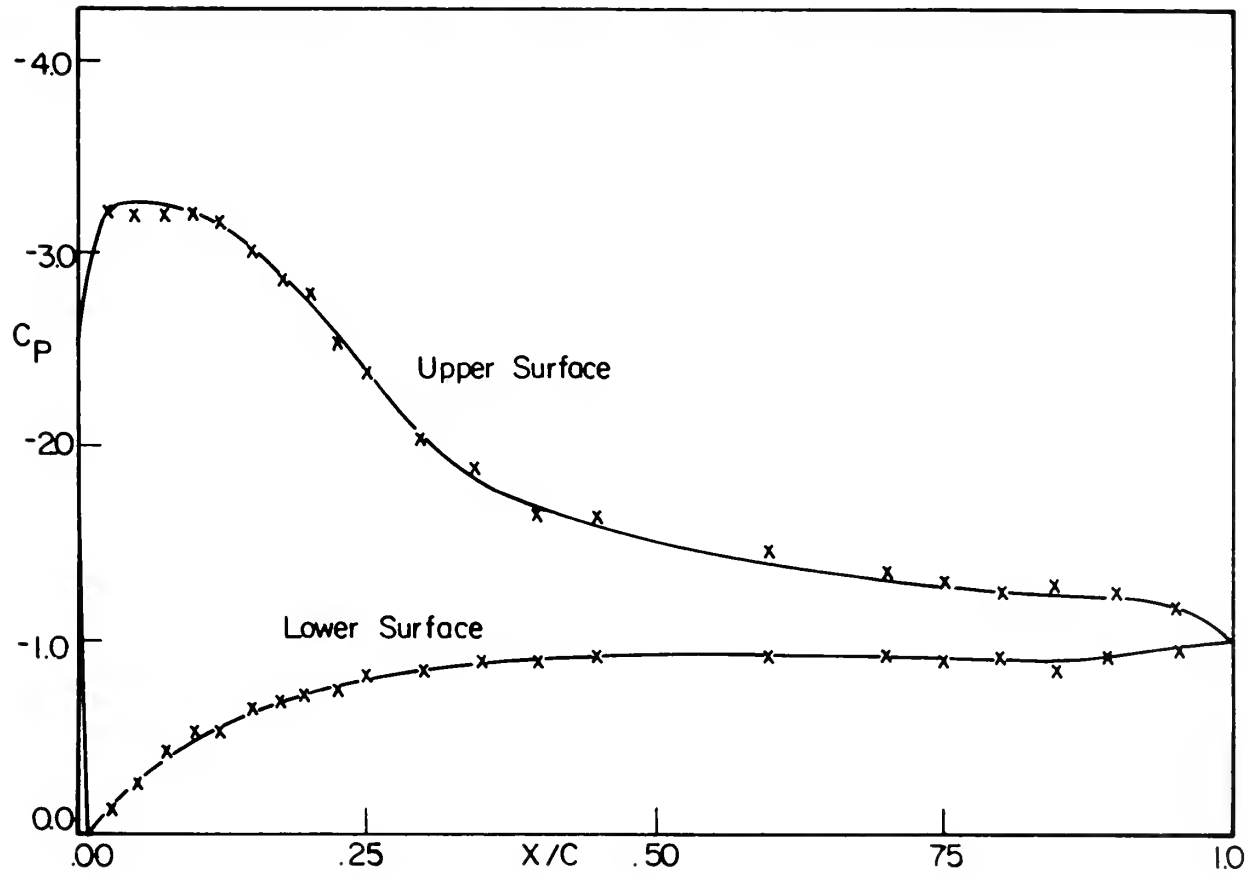

FIGURE 29

MEAN PRESSURE DISTRIBUTION ON AIRFOIL

$\frac{u'_{MAX}}{U}$ =.24 α = 10° f = 94 HERTZ

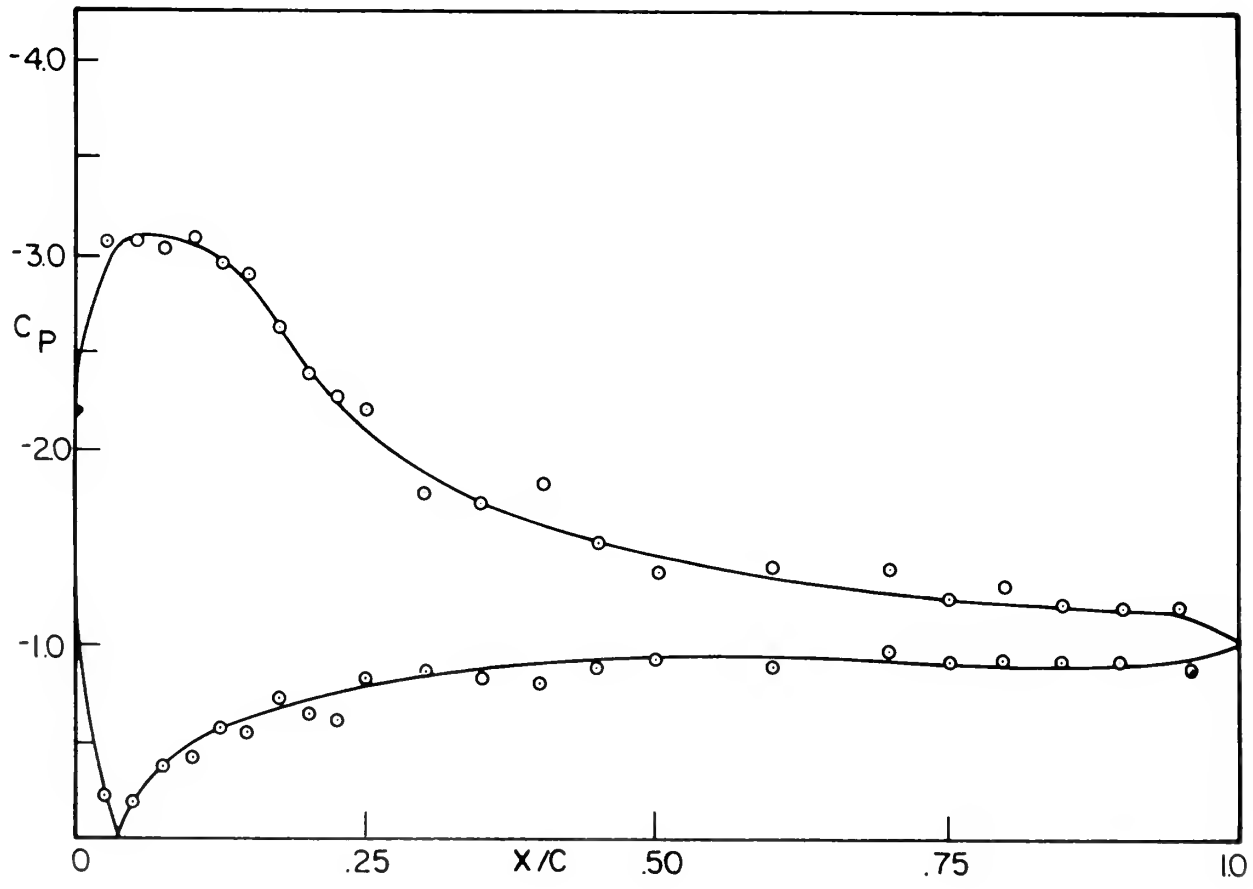

FIGURE 30

MEAN PRESSURE DISTRIBUTION ON AIRFOIL

$\frac{u'_{MAX}}{u} = .10$ $\alpha = 10°$ f = 128 HERTZ

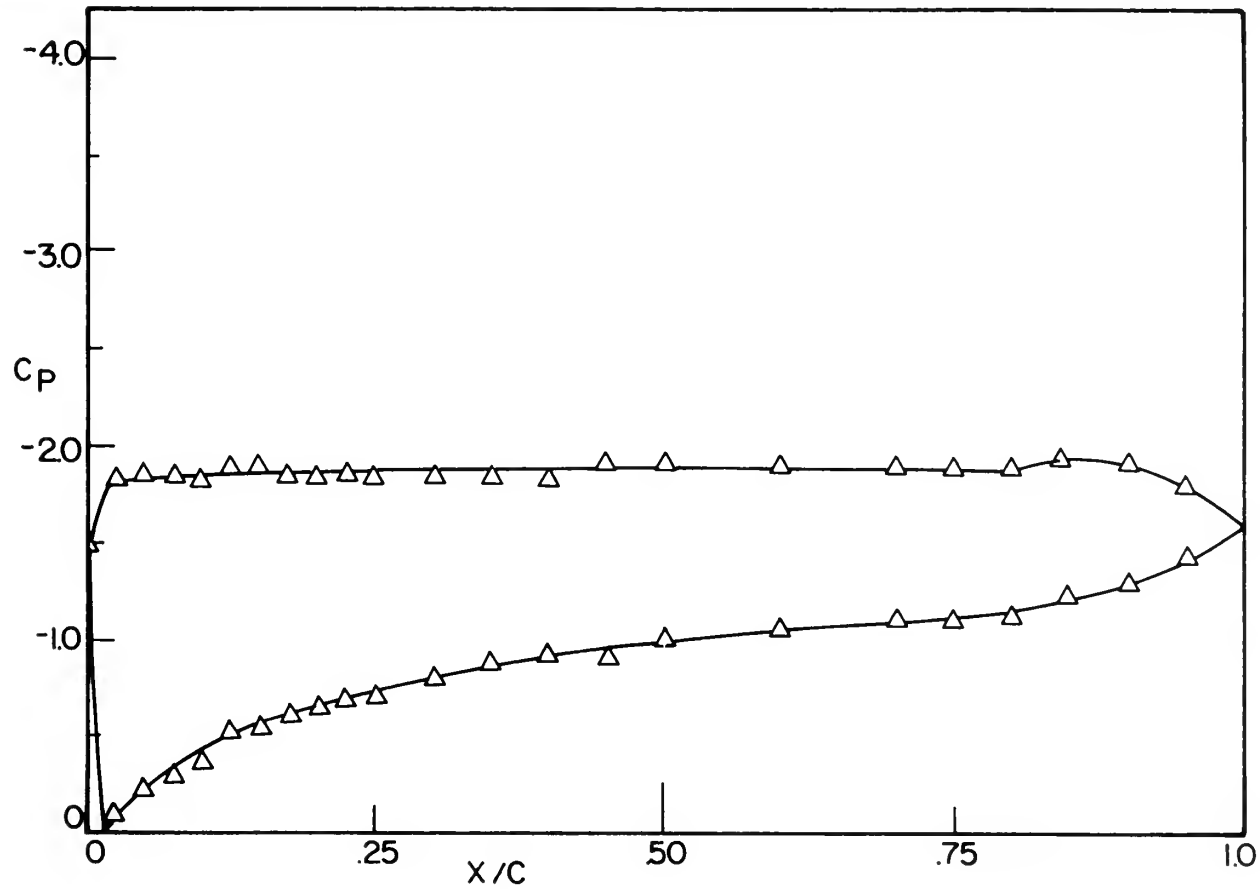

FIGURE 31

MEAN PRESSURE DISTRIBUTION ON AIRFOIL
$\alpha = 20°$ STEADY FLOW

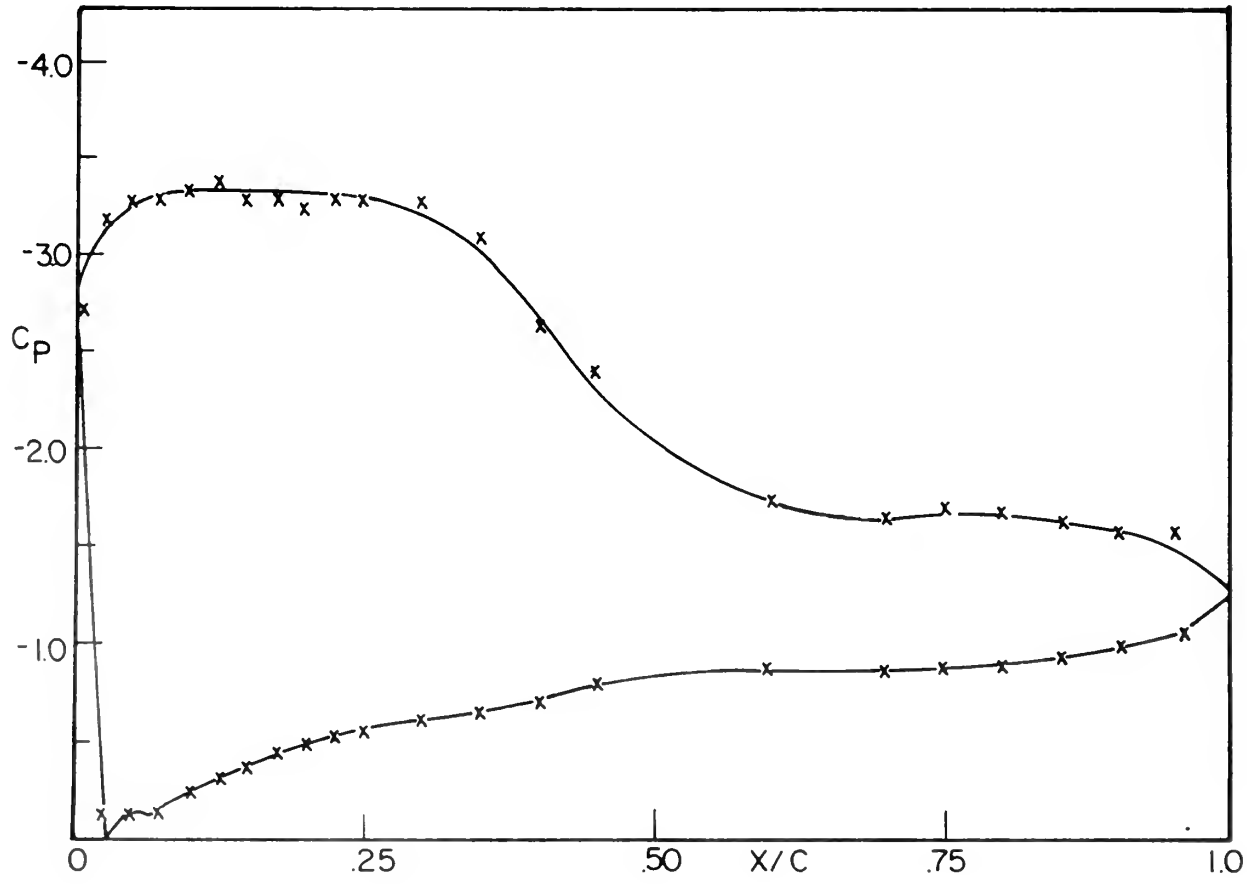

FIGURE 32

MEAN PRESSURE DISTRIBUTION ON AIRFOIL

$\frac{u'_{MAX}}{u}$ =.10 α =20° f = 94 HERTZ

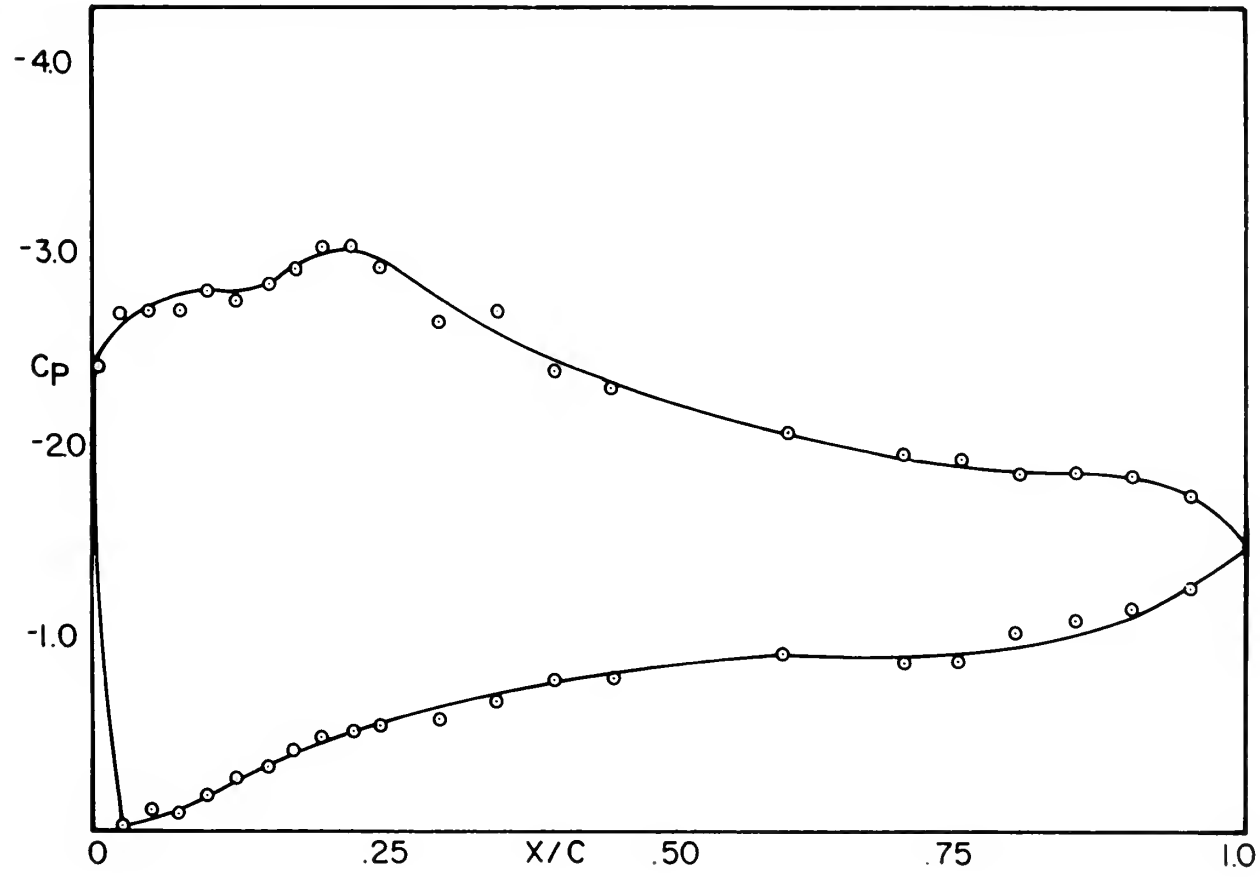

FIGURE 33

MEAN PRESSURE DISTRIBUTION ON AIRFOIL

$\frac{u'_{MAX}}{u}$ =.10 α =20° f = 128 HERTZ

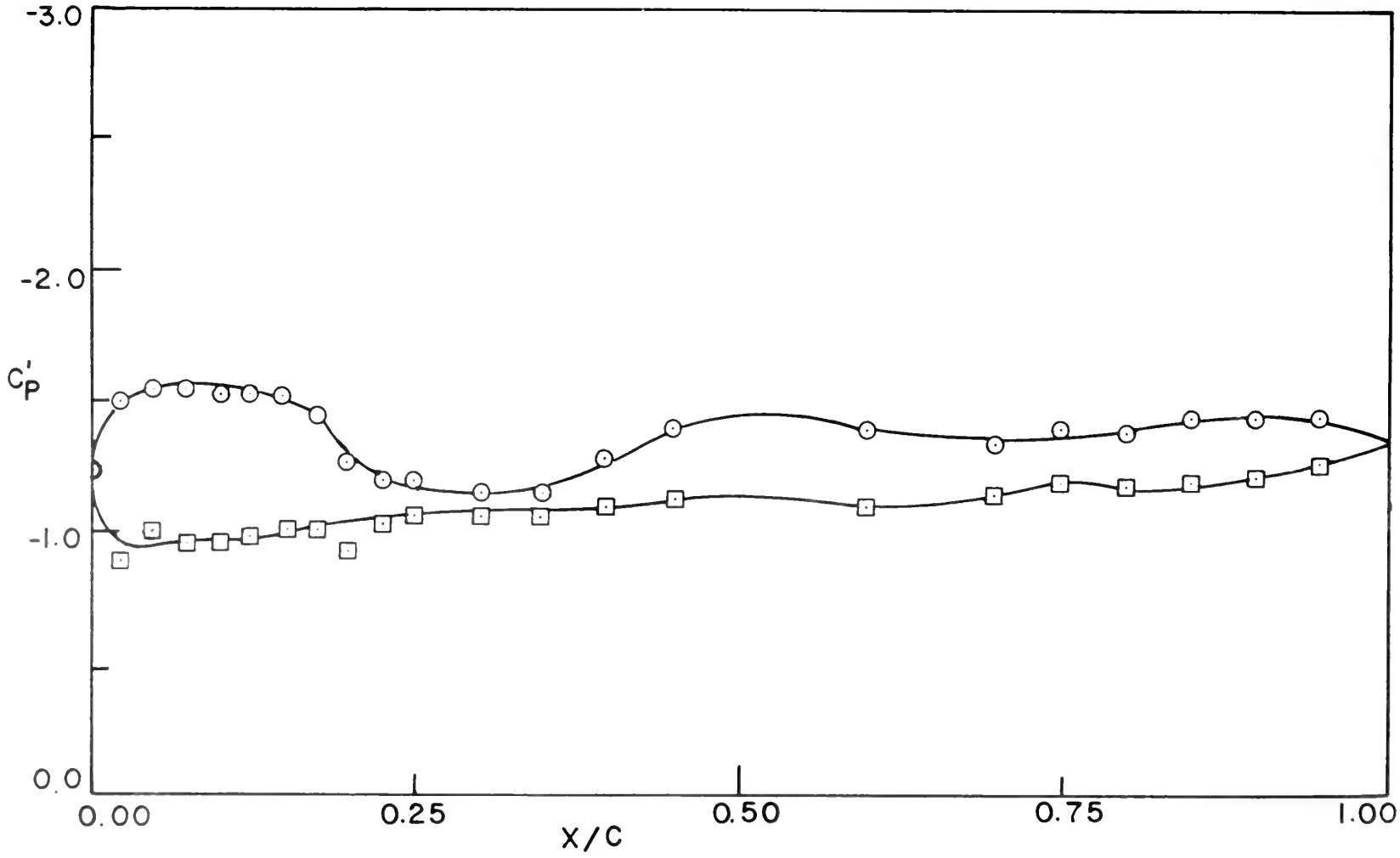

FIGURE 34. RMS PRESSURE DISTRIBUTION ON AIRFOIL

$\frac{U'_{max}}{U} = 0.10$ $\alpha = 20°$ f = 128 HERTZ

the oscillating components to the pressure remained of the same order from leading edge to trailing edge on the upper surface. They were also relatively constant on the lower surface but of lesser magnitude.

IV. CONCLUSIONS AND RECOMMENDATIONS

A. CONCLUSIONS

Three major observations can be made from the analysis of the experimental data:

1. The pressure in general leads the velocity in phase. The phase shift in the pressure waveform tends to increase with increasing chordwise dimension.

2. Second order and possibly higher harmonics are introduced in the pressure waveforms, possibly due to the nonlinearities inherent to the equations of motion.

3. The mean normal force coefficient was significantly larger in oscillating flow than in steady flow at the frequencies and angles of attack investigated. A hot wire probe above each pressure tap could be used to determine whether separation or a turbulent boundary layer were present. This information would resolve the question of the mechanism of separation advanced above.

B. RECOMMENDATIONS

Making each pressure reading by physically disconnecting each tube and reconnecting to another tube is very slow and clumsy. Some type of scanner valve, either manual or electrically driven, would greatly reduce time to take data.

A magnetic tape recorder could be used to record data which would be digitized and fed into a computer in order to obtain instantaneous lift. This would also overcome the problem of finding phase shifts.

APPENDIX A

TRANSDUCER CALIBRATION PROCEDURES

Proximity Detector Calibration

The proximity detector was calibrated to insure that the output was linear and the noise level low, and to determine if surrounding metal had any effect on the output. An existing calibration holder was modified for this purpose.

At one end of the calibration holder was a micrometer. The other end held the probe. Either of two fittings, a brass collar or a plexiglass collar with a circle of 0.003 inch brass foil cemented on its face, could be fastened to the end of the micrometer. The plexiglass was used to isolate the brass foil in order to compare the output with that from a solid piece of brass. A typical set-up for this calibration is shown in Figure 35.

For the calibration, one of the probes was placed so its face was just touching that of the collar on the micrometer. As the micrometer was backed off and the distance between collar and probe increased, the D.C. voltage output and R.M.S. voltage noise level for each .001 inch increment were recorded.

It was determined that the proximity detector output was linear. It was also observed that nearby metallic objects do have an effect on the voltage output. The calibration curve may be shifted up or down and its slope changed slightly depending on the mass of metal in the vicinity of the probe.

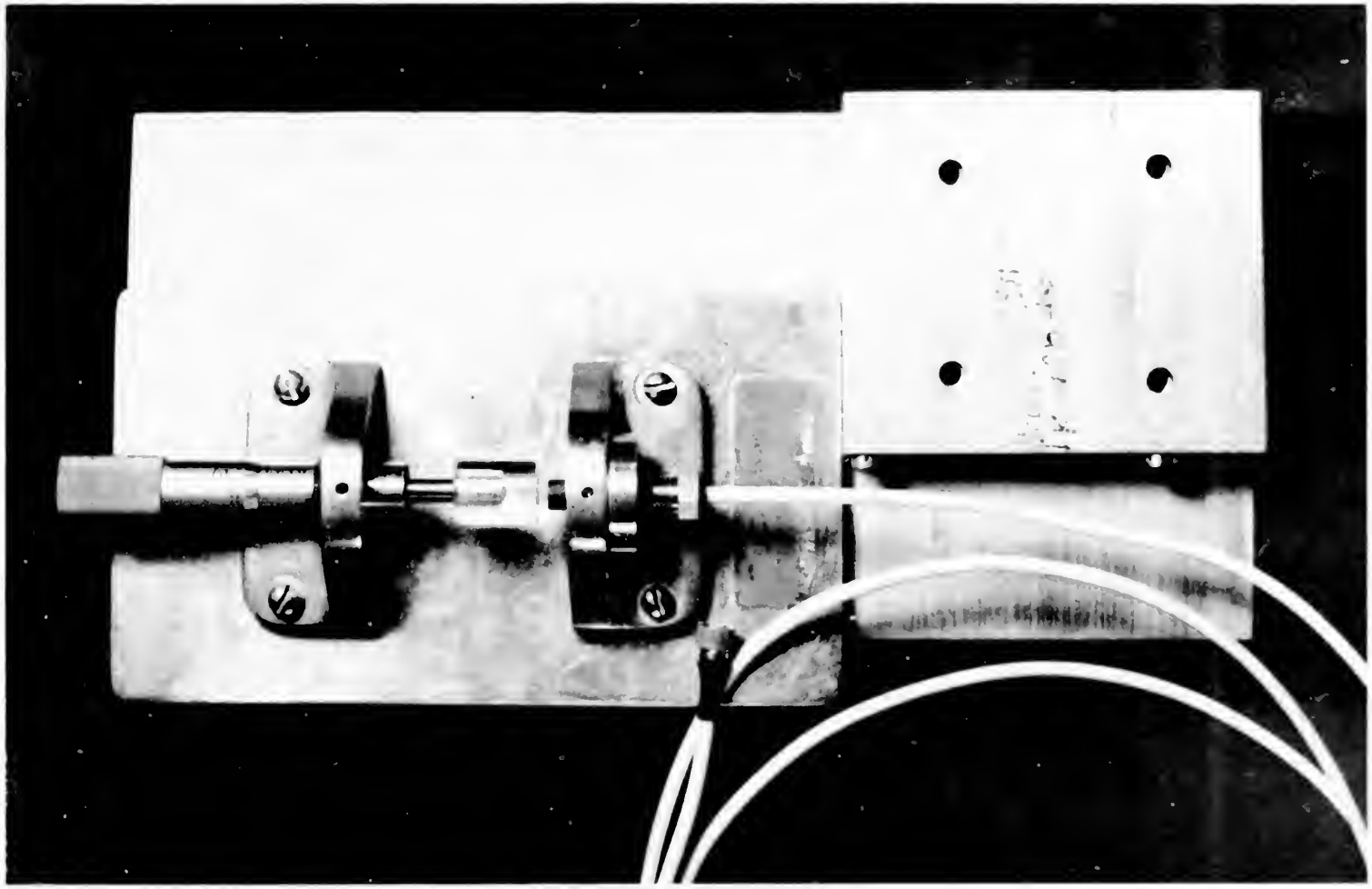

FIGURE 35. PROXIMITY DETECTOR CALIBRATION HOLDER

It was for this reason that a plexiglass spacer was placed in the transducer housing in order to reduce the effect the housing might have on the output. The results are summarized in Figure 36.

Static Calibration

The procedure for static calibration was the same as that employed by Johnson [Ref. 6]. Both transducers were set in the region of -3.0 volts D.C. output since the noise level in this region was small and the output would be linear with respect to diaphragm deflection. The results are given in Figure 9.

Dynamic Calibration

Dynamic calibration was also carried out using the procedure of Johnson [Ref. 6]. The results from his work were used to select the inside tube diameter and tube length for this investigation. The stainless steel tubing used in the model was .0625 inches O.D., .047 inches I.D., and 24 inches long. This same length of tubing plus 13.5 inches of plastic tubing (.049 inches I.D.) were used to connect the pressure chamber to the transducer in order to simulate the actual experimental conditions. Two spacing washers (total thickness of 0.015 inches) were used in the transducer housing.

Both transducers were mounted in the calibration chamber for the first step in dynamic calibration. The values of phase difference and R.M.S. voltages for both transducers were recorded at 5 hertz increments from 10 to 300 hertz and 10 hertz increments from 300 to 400 hertz. The dynamic

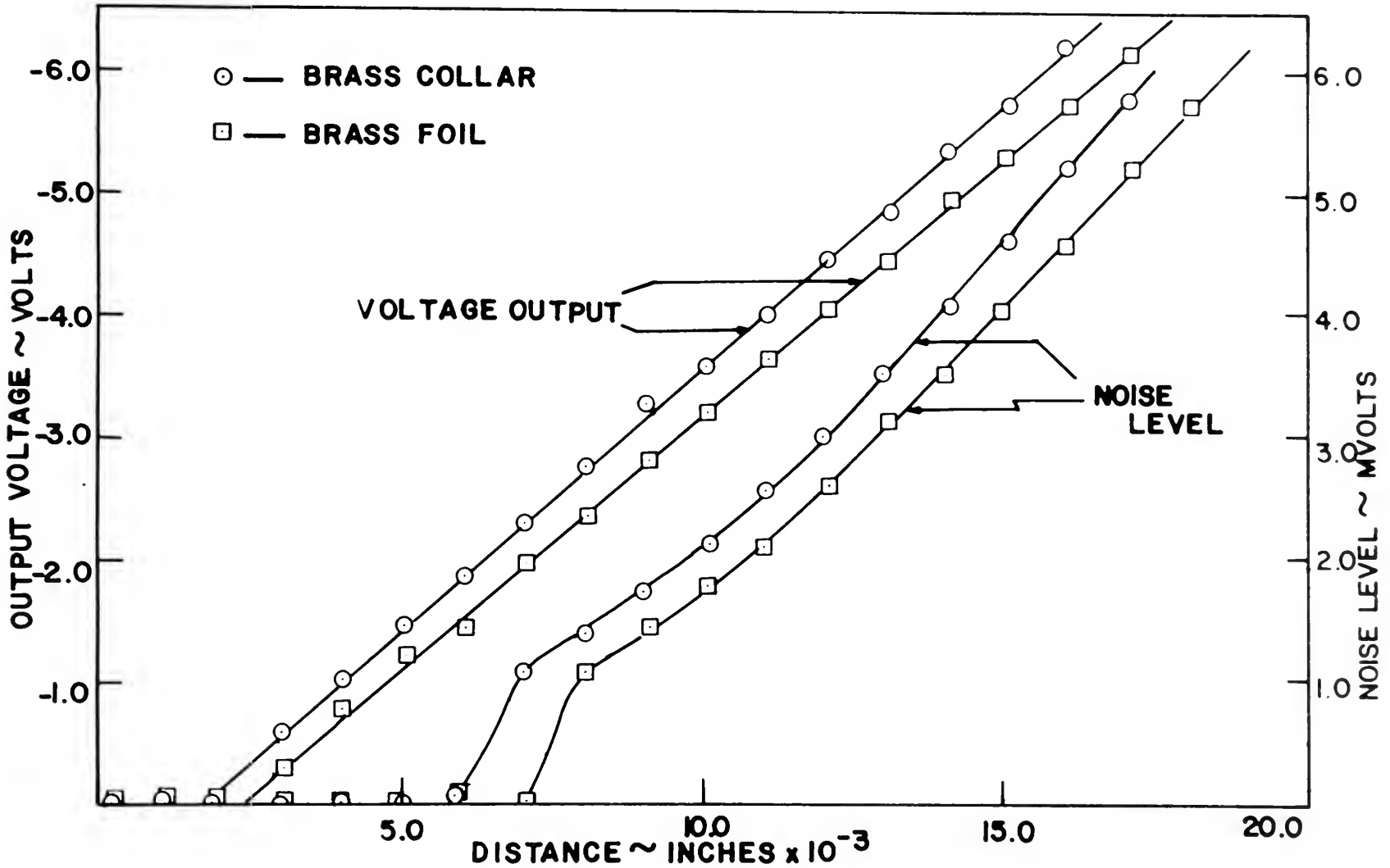

FIGURE 36. PROXIMITY DETECTOR CALIBRATION CURVES

responses of the two transducers were identical in relation to phase but the R.M.S. values differed uniformly by .738.

The next phase in calibration was to remove transducer #1 from the calibration chamber and reconnect it to the chamber through the steel and plastic tubing. Comparisons were then made of the dynamic characteristics of the two transducers. Dynamic gain and phase shift are defined as in Figure 37. The dynamic gain through the tubing was calculated by dividing the ratio of the transducer outputs by .738. The dynamic calibration curve is shown in Figures 10 and 11.

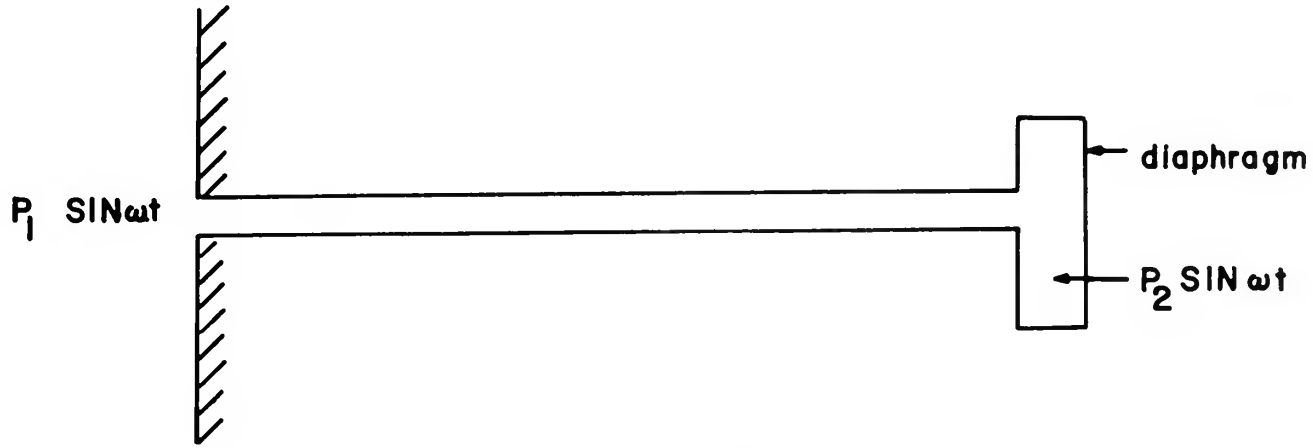

A. DYNAMIC GAIN $\equiv \frac{P_2}{P_1} = f(\omega)$

B. PHASE LAG = $\phi = g(\omega)$

FIGURE 37. PRESSURE MEASURING SYSTEM

APPENDIX B. TABLES OF EXPERIMENTAL DATA

TABLE I

PHASE SHIFT DATA

f = hertz

	α = 0°	α = 10°		α = 20°	
tap #	Δθ*	Δθ upper surface	Δθ lower surface	Δθ upper surface	Δθ lower surface
1	-20	-10	-10	13	13
2	-17	-10	-15	17	-40
3	-16	- 9	-12	13	-35
4	-12	-11	- 9	10	-35
5	- 8	- 7	- 5	8	-30
6	- 3	- 8	- 4	0	-35
7	0	- 8	1	-10	-35
8	2	- 9	5	-13	-25
9	10	-13	13	-20	-25
10	8	-18	10	-25	-18
11	10	-18	18	-27	-15
12	17	- 4	16	-30	- 7
13	23	-10	23	- 3	0
14	28	43	30	30	- 1
15	32	39	33	49	3
16	--	--	--	--	--
17	42	38	41	43	--
18	47	37	45	40	35
19	48	41	47	40	33
20	48	43	48	40	41
21	48	44	47	41	41
22	50	45	50	41	43
23	52	49	52	41	42

*Positive phase shifts indicate pressure leads velocity.

TABLE I (continued)

f = 128 hertz

	α = 0°	α = 10°		α = 20°	
tap #	Δθ*	Δθ upper surface	Δθ lower surface	Δθ upper surface	Δθ lower surface
1	13	15	15	20	20
2	15	18	14	21	13
3	14	18	14	21	12
4	16	16	14	20	13
5	17	14	15	17	13
6	17	13.5	15	15	13
7	16	13	15	15	14
8	18	16	16	15	15
9	19	20	17	16	14
10	20	22	17	17	15
11	20	24	18	20	16
12	21.5	26	20	23	17
13	23	28	20	30	17
14	24	30	21	24	18
15	25	30	22	27	19
16	--	--	--	--	--
17	29	30	27	26	23
18	31	32	28	25	26
19	32.5	33	30	24	27
20	35	34	31	24	29
21	35	34	31	24	29
22	36	35	32	26	31
23	37	36.5	33	27	34

*Positive phase shifts indicate pressure leads velocity.

TABLE II

MEAN PRESSURE COEFFICIENTS

$\alpha = 0°$

tap #	f = 128 hertz		f = 94 hertz		steady flow	
	ΔV	C_p	ΔV	C_p	ΔV	C_p
1	.000	.000	.005	.171	.002	.068
2	.035	1.195	.039	1.332	.041	1.400
3	.036	1.230	.042	1.434	.040	1.366
4	.038	1.298	.042	1.434	.040	1.366
5	.038	1.298	.041	1.400	.041	1.400
6	.038	1.298	.041	1.400	.041	1.400
7	.039	1.332	.040	1.366	.041	1.400
8	.039	1.332	.040	1.366	.040	1.366
9	.038	1.298	.040	1.366	.040	1.366
10	.041	1.400	.040	1.366	.040	1.366
11	.038	1.298	.043	1.469	.041	1.400
12	.038	1.298	.042	1.434	.040	1.366
13	.039	1.332	.041	1.400	.040	1.366
14	.037	1.264	.039	1.332	.039	1.332
15	.037	1.264	.039	1.332	.038	1.297
16	.032	1.093	.036	1.230	.037	1.263
17	.037	1.264	.035	1.195	.035	1.195
18	.031	1.059	.033	1.127	.032	1.093
19	.025	.854	.032	1.093	.030	1.024
20	.036	1.230	.031	1.058	.031	1.058
21	.029	.990	.029	.990	.030	1.024
22	.024	.820	.029	.990	.029	.990
23	.024	.820	.030	1.024	.029	.990

TABLE II (continued)

α = 10° (upper surface)

tap #	f = 128 hertz		f = 94 hertz		steady flow	
	ΔV	C_p	ΔV	C_p	ΔV	C_p
1	.069	2.357	.072	2.459	.044	1.503
2	.091	3.108	.093	3.176	.066	2.254
3	.090	3.074	.093	3.176	.060	2.049
4	.089	3.040	.093	3.176	.059	2.015
5	.091	3.108	.093	3.176	.060	2.049
6	.087	2.971	.091	3.108	.060	2.049
7	.086	2.938	.087	2.971	.060	2.049
8	.077	2.630	.082	2.800	.060	2.049
9	.070	2.391	.081	2.766	.061	2.083
10	.067	2.288	.074	2.527	.058	1.981
11	.065	2.220	.070	2.391	.055	1.878
12	.052	1.776	.060	2.049	.056	1.913
13	.051	1.742	.054	1.844	.054	1.844
14	.053	1.810	.049	1.673	.052	1.776
15	.045	1.537	.047	1.605	.051	1.742
16	.040	1.366	----	-----	.048	1.639
17	.041	1.400	.041	1.400	.046	1.571
18	.041	1.400	.039	1.332	.042	1.434
19	.036	1.230	.038	1.298	.041	1.400
20	.038	1.298	.037	1.264	.041	1.400
21	.035	1.195	.037	1.264	.040	1.366
22	.035	1.195	.036	1.230	.038	1.298
23	.035	1.195	.034	1.161	.038	1.298

TABLE II (continued)

$\alpha = 10°$ (lower surface)

tap #	f = 128 hertz		f = 94 hertz		steady flow	
	ΔV	C_p	ΔV	C_p	ΔV	C_p
1	.059	2.015	.065	2.220	.050	1.710
2	.007	.241	.005	.173	.005	.173
3	.006	.202	.008	.274	.008	.274
4	.011	.381	.013	.444	.011	.381
5	.012	.413	.015	.515	.014	.487
6	.017	.587	.015	.515	.015	.515
7	.016	.555	.019	.654	.018	.617
8	.021	.721	.020	.687	.020	.687
9	.019	.654	.021	.724	.022	.752
10	.018	.615	.022	.759	.022	.759
11	.024	.826	.024	.826	.023	.792
12	.025	.854	.025	.854	.022	.752
13	.024	.826	.026	.891	.027	.923
14	.024	.826	.026	.891	.027	.923
15	.026	.891	.027	.923	.026	.891
16	.027	.923	----	----	.028	.964
17	.026	.894	.027	.923	.027	.923
18	.028	.964	.027	.923	.028	.964
19	.027	.923	.026	.891	.028	.964
20	.027	.923	.027	.923	.027	.923
21	.027	.923	.025	.854	.027	.923
22	.027	.923	.027	.923	.028	.964
23	.024	.826	.028	.964	.028	.964

TABLE II (continued

$\alpha = 20°$ (upper surface)

tap #	f = 128 hertz		f = 94 hertz		steady flow	
	ΔV	C_p	ΔV	C_p	ΔV	C_p
1	.075	2.564	.089	3.041	.052	1.783
2	.078	2.663	.092	3.142	.054	1.846
3	.079	2.701	.096	3.284	.054	1.846
4	.079	2.701	.096	3.284	.054	1.846
5	.082	2.803	.097	3.314	.054	1.846
6	.080	2.730	.099	3.382	.055	1.885
7	.083	2.833	.096	3.284	.055	1.885
8	.085	2.901	.096	3.284	.054	1.846
9	.088	3.012	.095	3.241	.054	1.846
10	.088	3.012	.096	3.283	.054	1.846
11	.085	2.901	.096	3.283	.054	1.846
12	.077	2.636	.096	3.283	.054	1.846
13	.078	2.661	.090	3.074	.054	1.846
14	.070	2.394	.077	2.636	.054	1.846
15	.067	2.291	.070	2.394	.055	1.885
16	----	-----	----	-----	----	-----
17	.060	2.056	.051	1.742	.055	1.885
18	.057	1.954	.048	1.641	.055	1.885
19	.056	1.913	.049	1.675	.055	1.885
20	.054	1.842	.049	1.675	.055	1.885
21	.054	1.842	.047	1.616	.057	1.951
22	.053	1.813	.046	1.571	.056	1.913
23	.051	1.741	.046	1.571	.052	1.782

TABLE II (continued)

α = 20° (lower surface)

tap #	f = 128 hertz		f = 94 hertz		steady flow	
	ΔV	C_p	ΔV	C_p	ΔV	C_p
1	.068	2.564	.074	2.539	.038	1.302
2	-.001	-0.038	.004	.143	.003	.107
3	.003	.107	.004	.143	.007	.244
4	.003	.107	.004	.143	.009	.316
5	.006	.205	.007	.244	.011	.389
6	.008	.277	.009	.316	.015	.518
7	.010	.342	.011	.389	.016	.557
8	.012	.413	.013	.446	.018	.614
9	.014	.485	.014	.485	.019	.659
10	.015	.518	.015	.518	.020	.681
11	.016	.557	.016	.557	.021	.722
12	.017	.583	.018	.614	.023	.795
13	.020	.687	.019	.659	.025	.861
14	.023	.795	.020	.687	.027	.922
15	.023	.795	.023	.795	.027	.922
16	----	----	----	----	----	----
17	.027	.922	.025	.861	.030	1.063
18	.025	.861	.025	.861	.032	1.097
19	.026	.892	.026	.892	.032	1.097
20	.030	1.021	.026	.892	.033	1.125
21	.031	1.061	.027	.922	.036	1.231
22	.033	1.139	.029	.990	.038	1.302
23	.036	1.235	.031	1.061	.042	1.431

TABLE III

UNSTEADY PRESSURE COEFFICIENTS

$\alpha = 0°$

tap #	f = 128 hertz		f = 94 hertz	
	ΔV	C'_p	ΔV	C'_p
1	2.21	1.51	2.21	1.51
2	2.31	1.58	1.80	1.23
3	2.38	1.63	1.80	1.23
4	2.34	1.60	1.75	1.19
5	2.33	1.59	1.77	1.21
6	2.32	1.58	1.74	1.19
7	2.32	1.58	1.77	1.21
8	2.31	1.58	1.79	1.22
9	2.20	1.50	1.62	1.11
10	2.36	1.61	1.82	1.24
11	2.35	1.60	1.87	1.27
12	2.33	1.59	1.86	1.27
13	2.31	1.58	1.88	1.28
14	2.33	1.59	1.93	1.32
15	2.33	1.59	1.92	1.31
16	----	----	----	----
17	2.30	1.57	1.95	1.33
18	2.25	1.54	2.02	1.38
19	2.25	1.54	2.10	1.43
20	2.25	1.54	2.02	1.38
21	2.32	1.58	2.00	1.37
22	2.21	1.51	1.99	1.36
23	2.18	1.49	2.05	1.40

TABLE III (continued)

α = 10°			f = 94 hertz	
tap #	upper surface		lower surface	
	ΔV	C'_p	ΔV	C'_p
1	1.75	1.19	1.75	1.19
2	2.30	1.57	1.32	0.90
3	2.30	1.57	1.48	1.01
4	2.29	1.56	1.42	0.97
5	2.30	1.57	1.44	0.98
6	2.29	1.56	1.48	1.01
7	2.15	1.47	1.48	1.01
8	1.95	1.23	1.49	1.02
9	1.74	1.19	1.40	0.96
10	1.76	1.20	1.54	1.05
11	1.79	1.22	1.58	1.08
12	1.69	1.15	1.57	1.07
13	1.70	1.16	1.56	1.06
14	1.94	1.32	1.64	1.12
15	2.10	1.43	1.66	1.13
16	----	----	----	----
17	2.03	1.39	1.61	1.10
18	1.98	1.35	1.70	1.16
19	2.08	1.42	1.76	1.20
20	2.05	1.40	1.75	1.19
21	2.12	1.45	1.79	1.22
22	2.12	1.45	1.78	1.22
23	2.15	1.47	1.89	1.29

TABLE III (continued)

α = 20°			f = 94 hertz	
tap #	upper surface		lower surface	
	ΔV	C'_p	ΔV	C'_p
1	2.07	1.41	2.07	1.41
2	2.60	1.78	1.08	0.74
3	2.65	1.81	1.09	0.74
4	2.65	1.81	1.11	0.76
5	2.60	1.78	1.14	0.78
6	2.60	1.78	1.16	0.79
7	2.50	1.71	1.17	0.80
8	2.50	1.71	1.17	0.80
9	2.15	1.47	1.07	0.73
10	2.35	1.60	1.20	0.82
11	2.15	1.47	2.18	1.49
12	1.90	1.30	1.21	0.83
13	1.70	1.16	1.22	0.83
14	1.75	1.19	1.27	0.87
15	1.85	1.26	1.27	0.87
16	----	----	----	----
17	2.15	1.47	1.30	0.89
18	2.30	1.57	1.31	0.89
19	2.30	1.57	1.38	0.94
20	2.33	1.59	1.40	0.96
21	2.40	1.64	1.42	0.97
22	2.25	1.57	1.44	0.98
23	2.25	1.57	1.47	1.00

TABLE III (continued

α = 10°			f = 128 hertz	
tap #	upper surface		lower surface	
	ΔV	C'_p	ΔV	C'_p
1	2.34	1.60	2.08	1.43
2	2.75	1.88	2.00	1.36
3	2.74	1.19	2.00	1.36
4	2.70	1.84	2.02	1.38
5	2.61	1.78	2.01	1.37
6	2.50	1.71	1.96	1.34
7	2.40	1.64	1.96	1.34
8	2.40	1.64	2.00	1.36
9	2.15	1.47	1.86	1.27
10	2.30	1.57	1.96	1.34
11	2.30	1.57	2.00	1.36
12	2.35	1.60	1.97	1.35
13	2.35	1.60	1.97	1.35
14	2.48	1.69	2.05	1.40
15	2.48	1.69	2.03	1.39
16	----	----	----	----
17	2.45	1.67	1.98	1.35
18	2.39	1.63	1.98	1.35
19	2.32	1.58	1.96	1.34
20	2.29	1.56	1.94	1.32
21	2.29	1.56	1.96	1.34
22	2.20	1.50	1.92	1.31
23	2.14	1.46	1.92	1.31

TABLE III (continued

$\alpha = 20°$			f = 128 hertz	
tap #	upper surface		lower surface	
	ΔV	C'_p	ΔV	C'_p
1	1.64	1.12	1.96	1.34
2	1.32	0.90	2.30	1.58
3	1.48	1.01	2.30	1.58
4	1.42	0.97	2.29	1.56
5	1.44	0.98	2.30	1.58
6	1.48	1.01	2.29	1.56
7	1.48	1.01	2.15	1.47
8	1.49	1.02	1.95	1.33
9	1.40	0.96	1.74	1.19
10	1.54	1.05	1.76	1.20
11	1.58	1.08	1.79	1.22
12	1.57	1.07	1.69	1.15
13	1.56	1.07	1.70	1.16
14	1.64	1.12	1.94	1.32
15	1.66	1.13	2.10	1.43
16	----	----	----	----
17	1.61	1.10	2.03	1.39
18	1.70	1.16	1.98	1.35
19	1.76	1.20	2.08	1.42
20	1.75	1.19	2.05	1.40
21	1.79	1.22	2.12	1.45
22	1.78	1.21	2.12	1.45
23	1.89	1.29	2.15	1.47

LIST OF REFERENCES

1. N.A.C.A. Technical Note Number 1326, Airfoil in Sinusoidal Motion in a Pulsating Stream, by J. Mayo Greenberg, June, 1947.

2. Isaacs, Rufus, "Airfoil Theory for Flows of Variable Velocity," Journal of the Aeronautical Sciences, v. 12, p. 113-117, January 1945.

3. Liiva, Jaan, Unsteady Aerodynamic and Stall Effects on Helicopter Rotor Blade Airfoil Sections, paper presented at Aerospace Sciences Meeting, 6th, New York, N.Y., January 1968.

4. Liiva, Jaan and Davenport, Franklyn J., Dynamic Stall of Airfoil Sections for High-Speed Rotors, paper presented at American Helicopter Society, Inc., Annual National Forum, 24th, Washington, D.C., May 1968.

5. National Aero- and Astronautical Research Institute Report NLR-TR F.238., Theoretical and Experimental Results for the Dynamic Response of Pressure Measuring Systems, by H. Bergh and H. Tijdeman, January 1965.

6. Johnson, R. B., A Technique for Measuring Unsteady Pressures, A.E. Thesis, Naval Postgraduate School, Monterey, California, September 1968.

7. Jacobs, G. K., Intensity Distribution in the Oscillating Turbulent Boundary Layer on a Flat Plate, M.S. Thesis, Naval Postgraduate School, Monterey, California, March 1968.

8. Despard, R., Laminar Boundary Layer Separation in Oscillating Flow, Ph.D. Thesis, Naval Postgraduate School, Monterey, California, June 1969.

INITIAL DISTRIBUTION LIST

		No. Copies
1.	Defense Documentation Center Cameron Station Alexandria, Virginia 22314	20
2.	Library, Code 0212 Naval Postgraduate School Monterey, California 93940	2
3.	Commander, Naval Air Systems Command Department of the Navy Washington, D. C. 20360	1
4.	Dean of Research Administration Naval Postgraduate School Monterey, California 93940	2
5.	Chairman, Department of Aeronautics Naval Postgraduate School Monterey, California 93940	1
6.	Prof. James A. Miller Department of Aeronautics Naval Postgraduate School Monterey, California 93940	1
7.	Lt. j.g. Terry J. Allen, USN 809 Moall Street Prescott, Arizona 86301	1

DOCUMENT CONTROL DATA - R & D

(Security classification of title, body of abstract and indexing annotation must be entered when the overall report is classified)

1. ORIGINATING ACTIVITY *(Corporate author)*
Naval Postgraduate School
Monterey, California 93940

2a. REPORT SECURITY CLASSIFICATION
Unclassified

2b. GROUP

3. REPORT TITLE
Pressure Distribution on an Airfoil in Oscillating Flow

4. DESCRIPTIVE NOTES *(Type of report and inclusive dates)*
Master's Thesis, June 1969

5. AUTHOR(S) *(First name, middle initial, last name)*
Terry Jon Allen

6. REPORT DATE	7a. TOTAL NO. OF PAGES	7b. NO. OF REFS
June 1969	76	8

8a. CONTRACT OR GRANT NO.	9a. ORIGINATOR'S REPORT NUMBER(S)
b. PROJECT NO.	
c.	9b. OTHER REPORT NO(S) *(Any other numbers that may be assigned this report)*
d.	

10. DISTRIBUTION STATEMENT
Distribution of this document is unlimited.

11. SUPPLEMENTARY NOTES	12. SPONSORING MILITARY ACTIVITY
	Naval Postgraduate School Monterey, California 93940

13. ABSTRACT

The effect of oscillating flow on the pressure distribution of a symmetrical airfoil was investigated experimentally employing a remote pressure transducer.

An open circuit wind tunnel utilizing rotating shutter blades downstream of the test section was used to create oscillating flow. Tests were run at two frequencies, as well as at steady flow, and three angles of attack.

The mean and unsteady pressure characteristics were recorded from which mean values of the normal force were determined. The results indicate that an airfoil at high angle of attack will produce more lift in oscillating flow than in steady flow.

14. KEY WORDS	LINK A		LINK B		LINK C	
	ROLE	WT	ROLE	WT	ROLE	WT
Oscillating Flow						
Unsteady Flow						